Stress-Driven Transposable Element De-repression Dynamics and Virulence Evolution in a Fungal Pathogen

Simone Fouché,[1,2] Thomas Badet,[2] Ursula Oggenfuss,[2] Clémence Plissonneau,[1] Carolina Sardinha Francisco,[1] and Daniel Croll ⬡ *,[2]

[1]Plant Pathology, Institute of Integrative Biology, ETH Zürich, Zürich, Switzerland

[2]Laboratory of Evolutionary Genetics, Institute of Biology, University of Neuchâtel, Neuchâtel, Switzerland

*Corresponding author: E-mail: daniel.croll@unine.ch.

Abstract

Transposable elements (TEs) are drivers of genome evolution and affect the expression landscape of the host genome. Stress is a major factor inducing TE activity; however, the regulatory mechanisms underlying de-repression are poorly understood. Plant pathogens are excellent models to dissect the impact of stress on TEs. The process of plant infection induces stress for the pathogen, and virulence factors (i.e., effectors) located in TE-rich regions become expressed. To dissect TE de-repression dynamics and contributions to virulence, we analyzed the TE expression landscape of four strains of the major wheat pathogen *Zymoseptoria tritici*. We experimentally exposed strains to nutrient starvation and host infection stress. Contrary to expectations, we show that the two distinct conditions induce the expression of different sets of TEs. In particular, the most highly expressed TEs, including miniature inverted-repeat transposable element and long terminal repeat-*Gypsy* element, show highly distinct de-repression across stress conditions. Both the genomic context of TEs and the genetic background stress (i.e., different strains harboring the same TEs) were major predictors of de-repression under stress. Gene expression profiles under stress varied significantly depending on the proximity to the closest TEs and genomic defenses against TEs were largely ineffective to prevent de-repression. Next, we analyzed the locus encoding the Avr3D1 effector. We show that the insertion and subsequent silencing of TEs in close proximity likely contributed to reduced expression and virulence on a specific wheat cultivar. The complexity of TE responsiveness to stress across genetic backgrounds and genomic locations demonstrates substantial intraspecific genetic variation to control TEs with consequences for virulence.

Key words: fungi, virulence, transcriptomics, transposable elements, stress.

Introduction

Transposable elements (TEs) are mobile genetic elements that were first discovered in maize (McClintock 1950) and propagate in genomes without apparent benefit to the host (Doolittle and Sapienza 1980). Uncontrolled spread of TEs is thought to have a fitness cost to the host due to the increased genome size and higher likelihood of deleterious, nonhomologous recombination events (Mita and Boeke 2016; Chuong et al. 2017). TEs are subdivided into two major categories according to their mechanism of replication, namely, class I TEs that transpose through an RNA intermediate (i.e., RNA transposons) and class II TEs that transpose through a cut-and-paste mechanism (i.e., DNA transposons). Both classes of TEs are expressed. Host genomes have coevolved with their TEs to suppress their expression (Slotkin and Martienssen 2007). These mechanisms include epigenetic silencing through histone modifications or DNA methylation, targeted mutagenesis, and small RNA interference. In order to

autonomously replicate in the genome, some TEs evolved or co-opted regulatory sequences to ensure their own transcription. As a consequence, the dispersed nature of TE regulatory sequences shapes the expression landscape of the genome (Mita and Boeke 2016; Chuong et al. 2017). Epigenetic silencing of the host genome and environmental triggers are major factors influencing TE transcription levels, although the underlying mechanisms are poorly understood.

Most TEs are transcriptionally and transpositionally quiescent (Yoder et al. 1997; Zilberman et al. 2007). However, environmental stimuli and stress, in particular, have been shown to trigger epigenetic de-repression of TEs resulting in the activation of insertional mutagenesis (Miousse et al. 2015). TE de-repression in response to stress is widely shared across eukaryotes (Bundo et al. 2014; Van Meter et al. 2014; Voronova et al. 2014; Romero-Soriano and Guerreiro 2016; Ryan et al. 2016; Zovoilis et al. 2016; Huang et al. 2017; Hummel et al. 2017; Shpyleva et al. 2018). De-repression of

TEs under stress usually impacts TE transcription levels and can increase transpositional activity (Dubin et al. 2018). The impact of stress on TEs is often mediated through changes in the epigenetic state of the genome (i.e., de-repression) (Horváth et al. 2017) or the activation by a transcription factor (Capy et al. 2000). Some TEs have stress response elements that are regulatory sequences activated in response to stress (Bucher et al. 2012; Casacuberta and González 2013). Stress response elements are most common in long terminal repeat (LTR) retrotransposons and have been identified in one family of miniature inverted-repeat transposable elements (MITEs) (Yasuda et al. 2013). The relationship between stress and TE activation is complex with some studies showing TEs being upregulated, some show TE repression and yet other studies show transient upregulation and then down-regulation following exposure to a stress (Horváth et al. 2017). Stress mostly impacts facultative heterochromatin (Trojer and Reinberg 2007), whereas constitutive heterochromatin is typically associated with gene-poor, TE-rich regions that maintain repression (Dillon 2004; Saksouk et al. 2015). The distribution of TE families or specific copies of a TE can be strongly correlated with the local chromatin state (Lanciano and Mirouze 2018). The epigenetic landscape influencing TE de-repression dynamics is a highly dynamic trait among closely related species (Niederhuth et al. 2016) but also showing significant variation within species (Barah et al. 2013).

TE responsiveness to stress potentially constitutes a major compound cost to the deleterious impact of stress on an organism. However, stress can induce both the activation and repression of TEs as was shown for different ecotypes of *Arabidopsis thaliana* exposed to cold stress (Barah et al. 2013). In yeast and human cells, TEs were found to be repressed in response to stress (Menees and Sandmeyer 1996; Trivedi et al. 2014). Another example in *A. thaliana*, the *ONSEN* (LTR) retrotransposon is activated in response to heat stress due to heat response factors recognizing a regulatory sequence in the promoter of the ONSEN transposon (Ito et al. 2011; Cavrak et al. 2014). As a consequence, ONSEN insertions into genic regions were shown to induce the transcriptional upregulation of neighboring genes in response to heat stress (Ito et al. 2011). Therefore, TEs are frequently reactivated in response to stress and their activation can introduce new TE copies into the genome with *cis*-regulatory elements or associated chromatin states that are responsive to stress, thereby rewiring the stress response network of the genome (Cowley and Oakey 2013; Galindo-González et al. 2017). Hence, the stress activation of TEs likely depends on the type of stress, the identity of the TE, and the genetic background of the host. Furthermore, TE activation may generate adaptive genetic variation and accelerate host stress adaptation.

TE de-repression dynamics in pathogens of plants show the hallmarks of a conflict between TE proliferation and host control. Insertions of TEs in pathogen genomes generate significant adaptive genetic variation through gene inactivation, gene copy-number variation and altered gene expression, and have been shown to play a role in the evolution of genes encoding proteins involved in host interaction (Croll and McDonald 2012; Seidl and Thomma 2017; Fouché et al. 2018). In fungi, TEs can also lead to genetic variation through repeat-induced point mutation (RIP), a genome defense mechanism that targets and mutates repetitive sequences (Selker 2002). In *Leptosphaeria maculans* for instance, leakage of RIP into neighboring regions contributes to the diversification of effector genes (Rouxel et al. 2011). During the infection of a host plant, the pathogen must overcome a number of severe stresses (Ferreira et al. 2006; Hernández-Chávez et al. 2017). Initially, the pathogen is exposed to nutrient stress on the surface of the plant (Derridj 1996). Once the pathogen enters the plant, host defenses stimulate the accumulation of toxic reactive oxygen species (Shetty et al. 2007). To face plant-induced stresses and promote disease, pathogens express virulence factors (i.e., effectors). The expression of effectors is often governed by de-repression of facultative heterochromatin (Connolly et al. 2013; Qutob et al. 2013; Chujo and Scott 2014; Soyer et al. 2014, 2015; Schotanus et al. 2015; Studt et al. 2016). Hence, infection stress incidentally serves as an epigenetic trigger for adaptive upregulation of effectors (Sánchez-Vallet et al. 2018). Importantly, regions of facultative heterochromatin encoding effectors overlap with TEs (Soyer et al. 2015; Seidl and Thomma 2017). This raises the possibility that the de-repression of TEs interacts with the expression of effectors.

Zymoseptoria tritici is the most important pathogen of wheat in Europe (Fones and Gurr 2015; Torriani et al. 2015). The pathogen's ability to infect host plants is largely determined by a complement of small proteins, most of them effectors, that manipulate the host physiology upon contact. Effector genes are frequently located in proximity to TEs and are highly upregulated during early, stressful conditions of the host infection (Rudd et al. 2015; Palma-Guerrero et al. 2016; Haueisen et al. 2019; Palma-Guerrero et al. 2017; Fouché et al. 2018; Plissonneau et al. 2018). Effectors are thought to become upregulated by de-repression of facultative heterochromatin (Soyer et al. 2015, 2019). Both facultative and obligate heterochromatins are highly enriched in TEs in *Z. tritici* (Schotanus et al. 2015). *Zymoseptoria tritici* has a very plastic genome consisting of 13 core and up to eight accessory chromosomes that are not fixed within the species (Goodwin et al. 2011). Accessory chromosomes frequently undergo chromosomal rearrangements with breakpoints colocalized with TE insertions (Croll et al. 2013; Plissonneau et al. 2016, 2018; Hartmann et al. 2017). Genes involved in pathogenicity and stress tolerance are frequently located in close proximity to TEs (Hartmann et al. 2017; Krishnan et al. 2018; Meile et al. 2018). Populations segregate over a thousand gene presence–absence polymorphisms and gene deletions are preferentially located in proximity to TEs (Hartmann et al. 2017; Plissonneau et al. 2018). Adaptation to specific wheat cultivars is governed by either the deletion or mutation of effector genes (Hartmann et al. 2017; Zhong et al. 2017; Meile et al. 2018). Importantly, some effector genes were shown to have undergone concurrent reductions in expression raising the possibility that the observed reconfigurations in TE content close to effectors made critical contributions to host adaptation.

In this study, we used transcriptome profiling to test for the impact of two major stress factors in the life-cycle of the pathogen on TE de-repression. We used a nutrient-rich culture medium as a nonstress environment and transferred the fungus to a nutrient-deprived medium that simulates starvation. Independently, we analyzed the fungal transcriptome at four distinct stages during the infection of wheat spanning the early symptomless stage, the peak of lesion formation, and the saprotrophic stage. The early stages expose the pathogen to substantial nutrient and host defense stress factors. We replicated the two stress experiments with four genetically distinct strains of Z. tritici to identify how the genetic background influences TE responsiveness. All strains have fully assembled genomes and have experimentally confirmed virulence differences. TEs showed the highest expression under nutrient stress, but the expression differed significantly between TE families and between genetic backgrounds. Infection stress led to a large number of TE families to be upregulated at the peak of the symptom development on wheat leaves. Next, we determined how the genomic location affected the expression of TEs and identified distinct de-repression patterns depending on the type of stress, the distance to the closest genes, and the impact of genomic defense mechanisms. Finally, we analyzed a locus segregating variation at a key effector gene involved in host adaptation for the impact of TE de-repression. We show that the insertion of specific TEs led to silencing and in turn promoting virulence.

Results

TE Landscape and Transcriptomic Response to Stress Conditions

We analyzed four strains of Z. tritici that differed significantly in the progression of infection and response to stress (Lendenmann et al. 2014, 2016; Palma-Guerrero et al. 2017). The most virulent strain (3D7) developed visible symptoms within 12 days post-infection (Palma-Guerrero et al. 2016). Strains 1A5 and 1E4 developed symptoms on average with a 2-day delay and strain 3D1 showed the slowest symptom progression (Palma-Guerrero et al. 2017; Stewart et al. 2018). Each strain has a fully assembled and annotated genome (Plissonneau et al 2018) with similar percentages of TEs 16.0–18.1% (fig. 1A). Of the 111 TE families identified previously in the reference genome of the species (Grandaubert et al. 2015), all families were present in 1A5, 110 were identified in 1E4 and 3D1, and 108 were found in 3D7. LTR-Gypsy elements were the most abundant in all of the strains making up between 5–7% of the genomes, followed by LTR-Copia and LINE-1 elements (fig. 1B). The TE content was highest in accessory chromosomes (14–21; fig. 1C). Chromosome 14 of strain 3D1 had the highest TE content (>40%). Despite the similarity in overall TE content between strains, TE superfamilies showed marked differences in their distribution across chromosomes (fig. 1C). SINE elements were only present on chromosome 5 for strain 1A5, 1E4, and 3D1 and on chromosome 3 for strain 3D7.

We analyzed the transcriptomic response to specific stress conditions by culturing the fungi first in nutrient-rich conditions, then analyzed the same strains growing in a minimal carbon source medium (i.e., starvation stress; fig. 2A). In parallel, we passaged all strains through an infection cycle on a wheat host (i.e., infection stress; fig. 2A). Infection stages were sampled at four time points (7, 12, 14, and 28 days post-infection). Across all conditions, we found that biological replicates clustered tightly together showing high stress reproducibility (supplementary fig. S2, Supplementary Material online). Gene expression profiles clustered mainly according to condition with early and late infection phases resembling nutrient starvation (fig. 2C). We analyzed the expression of putative virulence factors (i.e., effectors) and carbohydrate-active enzymes (CAZymes) in strain 3D7 in order to recapitulate the progression of the infection and impact of starvation. Overall, effector genes were upregulated during early infection stages (7–14 days post-infection; dpi) followed by downregulation at the final infection time point (supplementary fig. S3, Supplementary Material online). CAZymes are enzymes that digest carbohydrates and digest the plant cell walls, releasing nutrients for the pathogen. CAZymes differed widely in expression profiles with subsets showing upregulation during early infection stages, in nutrient-rich conditions and nutrient starvation, respectively (supplementary fig. S4, Supplementary Material online). Overall, stress conditions impose major gene expression profile changes consistent with the lifestyle transitions of the pathogen.

Differential Stress Response Dynamics of TEs across Environments

We analyzed TE expression across all conditions and strains using TETranscripts, which quantifies the expression abundance of a TE across all copies in the genome allowing for multiple read mapping. TE families differed substantially in expression profiles depending on the imposed stress condition (fig. 2B). A principal component analysis showed that the expression of TEs clustered according to the host genotype rather than stress condition (fig. 2D). Most TEs were expressed in most backgrounds and stress conditions (fig. 2E). The lowest percentage of expressed TEs was observed during early infection. We analyzed the relative expression of TEs versus genes expression and found that the highest relative TE expression occurred under nutrient-rich and starvation stress conditions (fig. 2F). The relative expression decreased with the progression of infection (fig. 2F).

The response of TEs to stress conditions was highly specific to individual TE families. In strain 3D7, two LTR-Gypsy element families and a TIR-Tc1-mariner element family were only upregulated during early infection (7–14 days post-infection; supplementary fig. S5B, Supplementary Material online). Similarly, in strain 3D1 four LTR-Gypsy element families were mainly upregulated early during infection (supplementary fig. S5A, Supplementary Material online). Two of these upregulated families were shared between the strains (LTR-Gypsy element families 6 and 9) and are the most infection stress-responsive elements. In 1A5 and 1E4, a shared TE element family (TIR-hAT element 1) was most highly expressed during
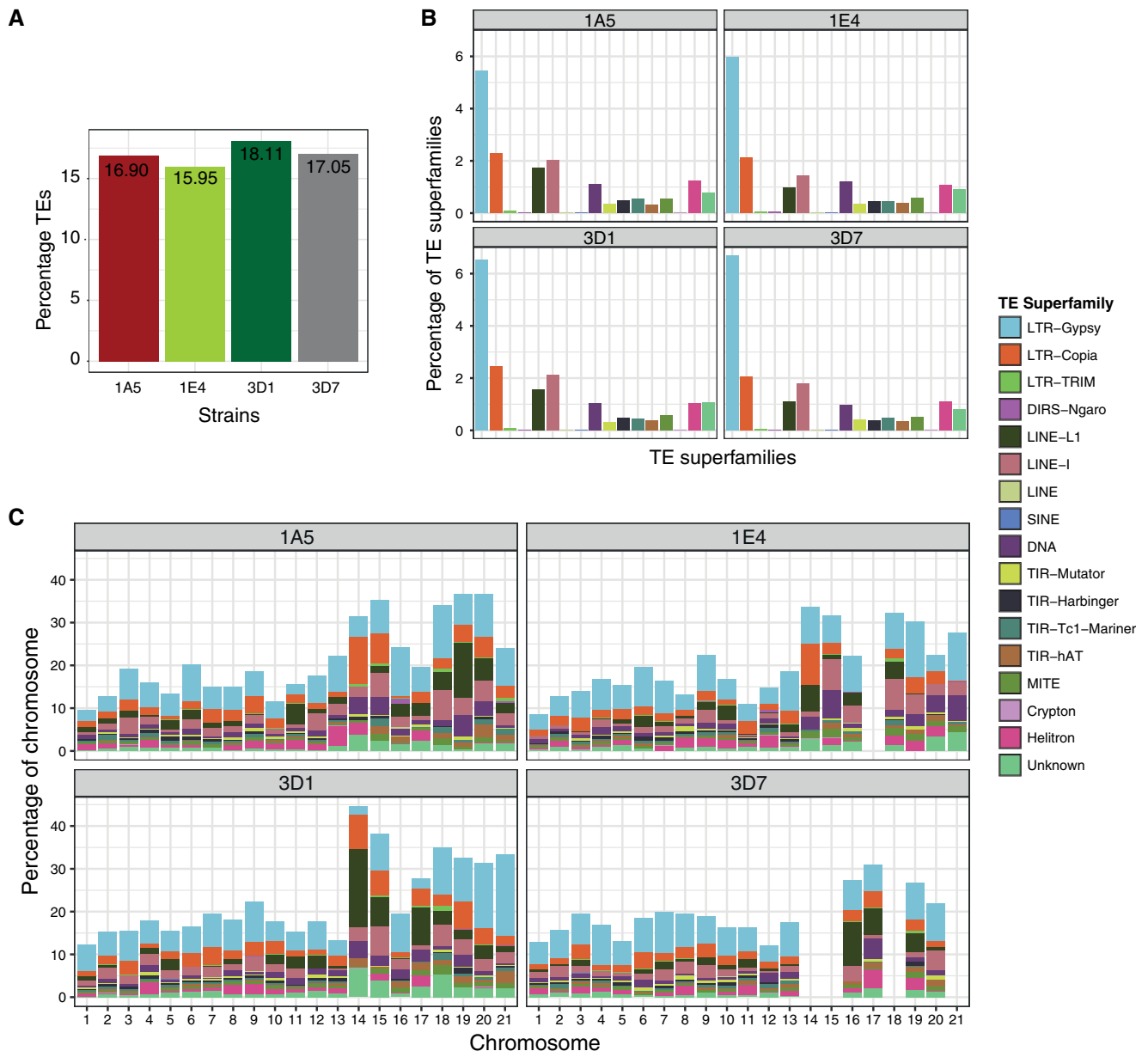
FIG. 1. TE composition of the completely assembled genomes of *Zymoseptoria tritici*. (*A*) The percentage TE in each genome. (*B*) The percentage of TE superfamilies in each strain. (*C*) The distribution of TE superfamilies as a percentage of the chromosomes for each strain.

starvation and mostly repressed during infection (supplementary fig. S5C and D, Supplementary Material online). Some TE families showed consistently high expression across all conditions suggesting generally weak genomic defenses against expression of this specific TE in comparison to other TEs that are only responsive to specific stress conditions (supplementary fig. S5A–D, Supplementary Material online). TE expression in all four strains was dominated by an MITE-Undine family (fig. 3), which is the most highly upregulated TE under nutrient starvation stress in all strains. The exception is strain 3D7 where the family was similarly expressed under nutrient rich conditions and starvation stress (fig. 3A). MITE-Undine is a nonautonomous element lacking coding regions. We were unable to identify the helper autonomous

element with the same terminal-inverted repeats (TIR). MITE-Undine was also the most abundant element in any of the four genomes (fig. 3B) with a copy number of 250–296. The mean number of TE copies per family in each genome was 29–32. The average distance of MITE-Undine to the nearest gene was 17.6–33.8 kb compared with 19.5–21.1 kb for all TEs (supplementary table S2, Supplementary Material online). The element was present on all chromosomes (fig. 3C for isolate 3D1) and contains target site sequences, TIR, and low-complexity regions (palindromes and tandem repeats; fig. 3D and supplementary file S1, Supplementary Material online). We found no evidence for the element in the genomes of the most closely related *Z. pseudotritici* and the more distantly related *Z. brevis*. However, *Z. ardabiliae* which
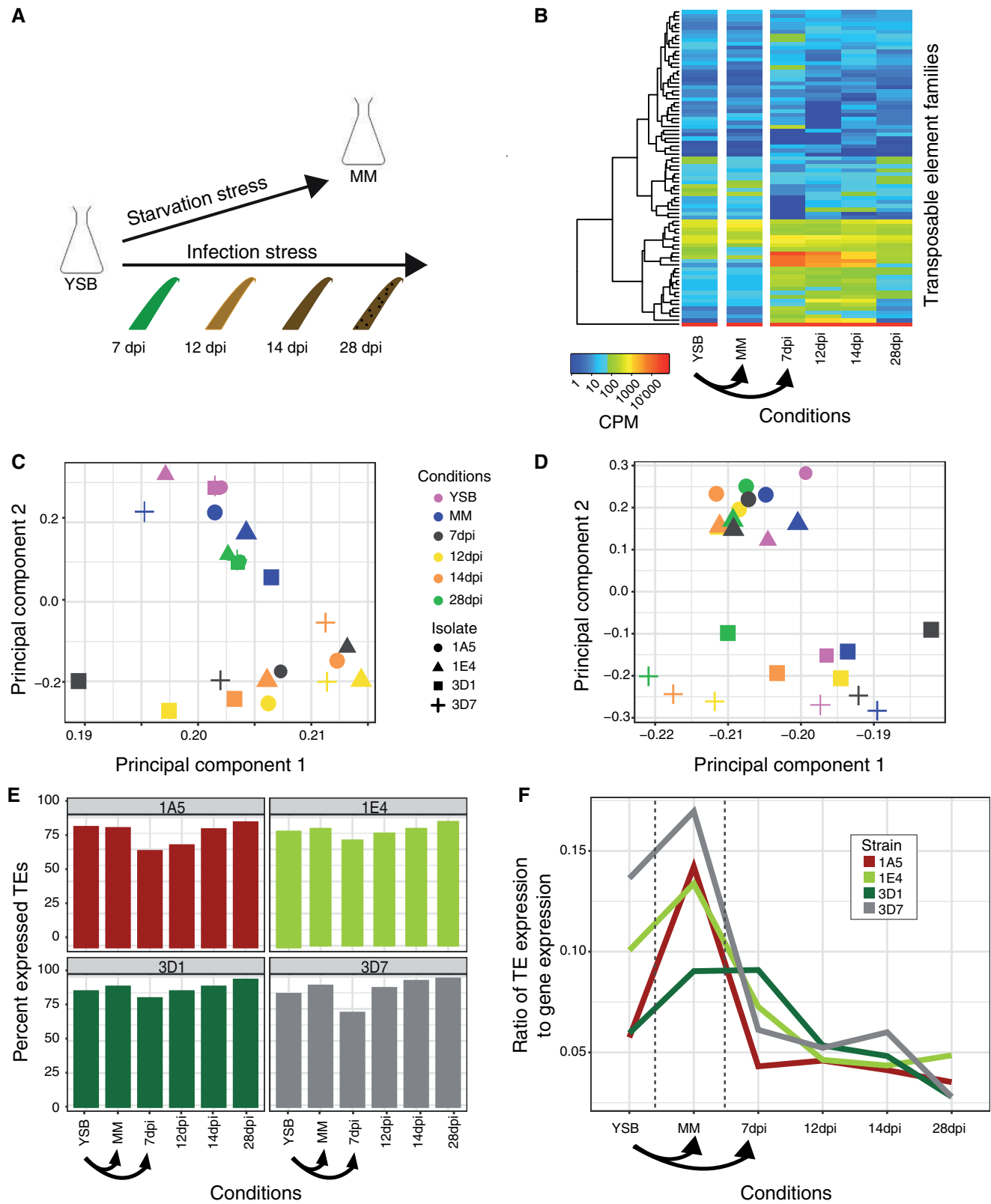
Fig. 2. Responsiveness of TE to different stresses. (A) Transcriptomes analyzed in response to nutrient and infection stress. (B) Heatmap showing expression of TE families in the strain 3D1. Principal component analyses of gene expression (C) and TEs (D) in the four strains. (E) The percentage of expressed TEs compared with all TEs for each condition. (F) Ratio of TE expression to gene expression. MM, nutrient poor media; YSB, nutrient rich media.
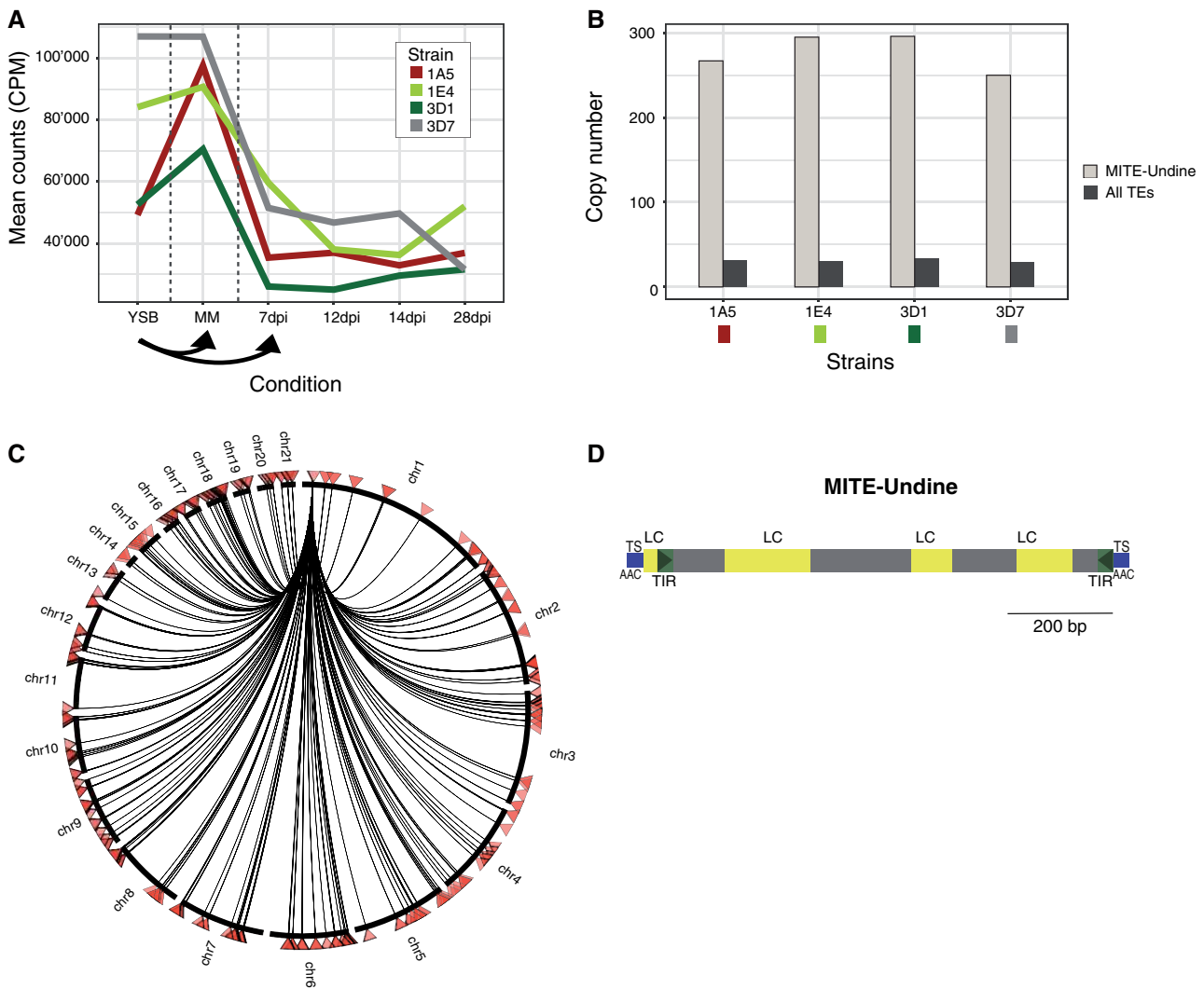
Fig. 3. Characterization of the high-copy and highly expressed MITE-Undine element. (*A*) The expression of MITE-Undine in CPM in all four strains. (*B*) The copy number of MITE-Undine compared with the mean copy number of all TEs. (*C*) Identification of MITE-Undine copies in the genome of 3D1. (*D*) Schematic of MITE-Undine with target site duplications (TS), TIR, and low complexity regions (LC). MM, nutrient poor media; YSB, nutrient rich media.

has an intermediate divergence time from *Z. tritici* harbors eight copies of the MITE-Undine.

TE and Gene Expression Dynamics as a Function of the Genomic Localization

To address the impact of physical proximity to TEs on gene expression patterns, we analyzed gene expression across stress conditions as a function of distance to the closest TE. Genes within 1 kb upstream or downstream of TEs were upregulated early during infection (7–14 dpi depending on the strain) compared with genes >1 kb away from TEs (fig. 4A and supplementary fig. S6, Supplementary Material online). Genes >1 kb away from TEs showed higher expression than genes <1 kb of TEs late in the infection (28 dpi). Genes with TE insertions showed consistently low levels of expression. Effector genes were overall closer to TEs than CAZymes, genes encoding secreted proteins or genes overall (fig. 4B and supplementary fig. S7, Supplementary Material online). Consistent with the proximity to TEs, effector genes were

strongly upregulated early during infection compared with other gene categories (fig. 4C and supplementary fig. S8, Supplementary Material online). Notably, the increase occurred first for 3D7, the strain with the most rapid infection progression (Palma-Guerrero et al. 2017) (supplementary fig. S8, Supplementary Material online). The increase occurred at 12 dpi and peaked at 14 dpi for the other three strains (supplementary fig. S8, Supplementary Material online).

Next, we analyzed TE expression responses to stress as a function of the distance to the closest genes. TE expression generally peaked for TEs at a mean distance of 15–20 kb to the closest gene for 3D1 and 3D7 and at 20–45 kb away from the closest gene for 1A5 and 1E4 (fig. 4D and E and supplementary fig. S9, Supplementary Material online). In strains 3D1 (fig. 4D) and 1E4 (supplementary fig. S9B, Supplementary Material online), TEs with a mean distance of within 1 kb of genes were upregulated during early infection. In 3D1, the upregulation at 7–14 dpi was primarily due to the expression of an LTR-*Gypsy* element, but also due to
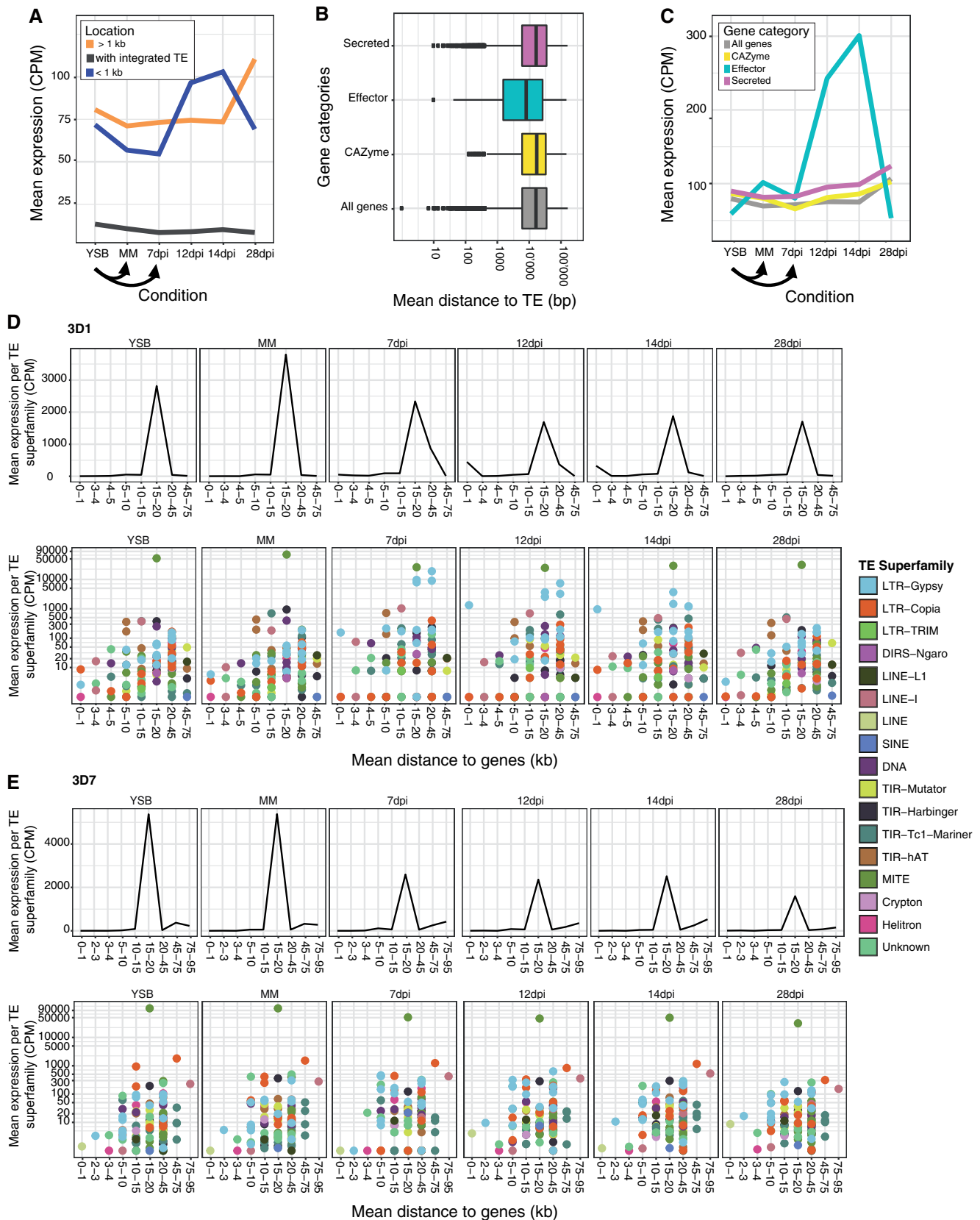
FIG. 4. Gene expression as a function of proximity to TEs in strain 3D1. (*A*) Expression of genes with inserted TEs, within 1 kb of the nearest TE or more than 1 kb from the nearest TE. (*B*) Mean distance between genes grouped by functional category. (*C*) Mean expression of genes grouped by functional category. TE expression responses to stress as a function of the distance to the closest genes in 3D1 (*D*) and 3D7 (*E*). Distance segments lacking TEs were omitted. MM, nutrient poor media; YSB, nutrient rich media.

the expression of a LTR-*Copia* element family at 14 dpi (fig. 4D). In 1E4, TEs with a mean distance within 1 kb of genes were also upregulated under nutrient stress, primarily due to the expression of an unknown element and an LTR-*Gypsy* element (supplementary fig. S9B, Supplementary Material online). In 3D7 and 1A5, TE families further away from genes were more strongly expressed (fig. 4E and supplementary fig. S9D, Supplementary Material online). Exceptions in 1A5 include TE families with a mean distance of 1–2 kb to the nearest gene, which were upregulated under all of the conditions due to the expression of two unknown element families and two LTR-*Gypsy* families (supplementary fig. S9D, Supplementary Material online). TE families with a mean distance of >45 kb away from the nearest gene showed upregulation under all conditions in strain 3D7, with a major peak at 12 dpi (fig. 4E). The most highly expressed families falling in this category were an LTR-*Copia* family at mean distance of 45–75 kb and MITE-Undine at 75–95 kb from the nearest gene.

Co-expression Networks of Genes and TEs across Stress Conditions

Many TEs in the *Z. tritici* genome are in close physical proximity to genes and may, hence, converge on similar epigenetic de-repression dynamics across stress conditions. To infer synchronicity of TE and gene expression, we performed clustering analyses to define profiles of TE and gene coregulation under stress. The analysis identified a total of 20 co-expression profiles, of which six were shared by all four strains and six were strain-specific. Eighteen co-expression profiles contained TEs but were not identified in all isolates (fig. 5A). Expression profiles included different kinetics of upregulation upon infection stress (see profiles 16–17–18–27–28–29–31–39) but also downregulation (see profiles 8–9–13–15–19–20–21–32–35) with various intermediary profiles (fig. 5A). Co-expression profiles included on average >98% of genes and up to 5% of TEs in each genome (fig. 5A). To infer the biological relevance of different co-expression clusters, we performed enrichment analyses of gene ontology (GO) terms. In total, 11, 7, 14, and 12 co-expression profiles showed significant enrichment for GO terms in strains 1A5, 1E4, 3D1, and 3D7, respectively (P-value < 0.05). Four co-expression profiles were found consistently enriched for GO terms in the four strains (profiles 8, 18, 32, and 36; fig. 5A and supplementary table S3, Supplementary Material online). These profiles included enrichment for hydrolase, phosphorylation and transcriptional activity, as well as carbohydrate metabolism, kinases, and DNA replication functions (fig. 5A and supplementary table S3, Supplementary Material online).

Both DNA and retrotransposons were coexpressed with genes. LTR-*Gypsy* elements were dominating co-expression profiles reflecting the abundance of the elements in the genomes. Among all four strains, the co-expression profiles displaying higher numbers of TE superfamilies were consistently those with a peak of expression early in the infection process (e.g., profile 18). TE and gene coregulation could be driven by shared epigenetic environments due to physical proximity and/or transcriptional leakage. To test for the effect of physical proximity, we analyzed the physical distance between coexpressed TEs and their closest coexpressed genes. In concordance with the previous global analysis, coexpressed genes with a peak of expression early upon infection are found closer to TEs. However, the closest distance between coexpressed genes and TEs within an expression profile is on average ten times longer than the distance of the closest coexpressed genes and TEs not in the same expression profile (fig. 5B). Therefore, TEs and coexpressed genes are not closer than TEs and genes that do not share an expression profile.

Impact of Genomic Defenses on TE Expression under Stress

Fungi evolved sophisticated genomic defenses that inactivate TE copies through the introduction of RIPs (Selker 2002). In order to determine how RIP may impact TE expression under stress, we analyzed mutational biases among genomic TE copies. Most TE families in all four genomes were affected by RIP (fig. 6A and supplementary fig. S11, Supplementary Material online). Only TE families in the LTR-TRIM superfamily and one family in the TIR-*Tc1-mariner* superfamily were not affected by RIP. In all strains, TEs in the TRIM family were among the most highly affected TEs. In 1A5, a family belonging to the TIR-*Tc1-mariner* superfamily is consistently expressed under all conditions (supplementary fig. S10A, Supplementary Material online). Similarly, LTR-*Gypsy* elements with strong RIP signatures were upregulated upon infection in the strains 1A5, 1E4, and 3D1 (supplementary fig. S11A, Supplementary Material online). Hence, most TE families affected by RIP are still expressed under at least some stress conditions.

TE Insertion Dynamics in Proximity to Genes

TE superfamilies showed substantial variation in their mean distance to the closest gene with most having a mean distance to the nearest gene of <25 kb (fig. 6B and supplementary fig. S12, Supplementary Material online). The closest TE superfamilies to genes were DIRS-*Ngaro* (2,867 bp) in 1A5, LINE (415 bp) in 1E4, LINE-*1* (7,457 bp) in 3D1, and LINE (832 bp) in 3D7 (supplementary table S4, Supplementary Material online). Next, we analyzed coding sequence disruptions across the genome and LTR-*Copia* elements were the most frequently inserted TEs into genes in all strains except 1A5 (fig. 6C; supplementary fig. S12A and table S5, Supplementary Material online). Singleton genes defined as present in only one of the four strains were the most frequently disrupted genes (fig. 6D and supplementary fig. S12B, Supplementary Material online). Genes with inserted TEs had a lower expression than genes without TEs (fig. 6E and supplementary fig. S12E, Supplementary Material online). Hereafter, we analyzed TE insertions in close proximity to genes. We found again that LTR-*Copia* elements were the most abundant elements with 108–132 copies (fig. 6F; supplementary fig. S12C and table S6, Supplementary Material online). Singleton genes most frequently had an integrated TE or were located within 1 kb from a TE, followed by accessory genes and core genes (fig. 6D and G and supplementary fig. S12B and D, Supplementary Material online).
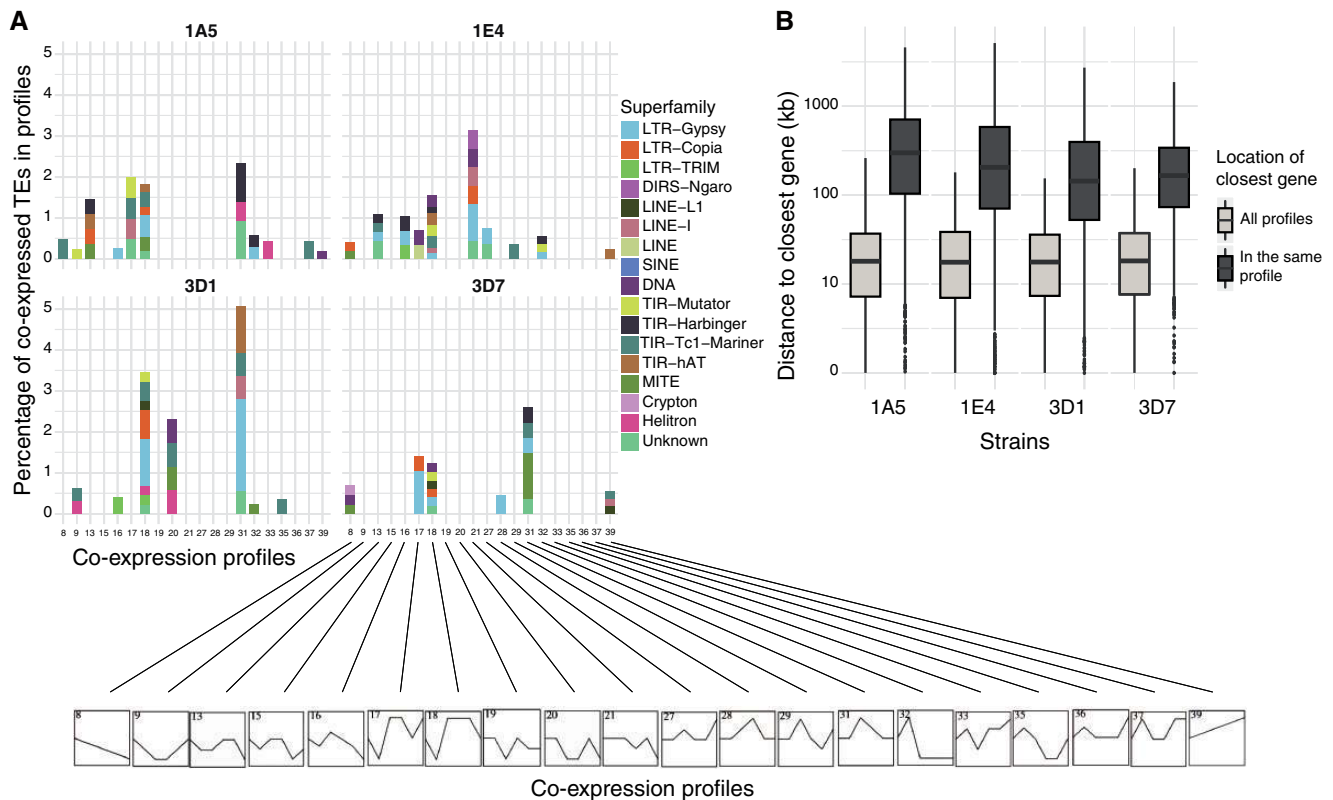
FIG. 5. Co-expression profiles of TEs and genes. (A) The percentage of TE families in each co-expression profile. (B) The distribution between TEs and coexpressed genes. TEs and coexpressed genes are not closer than TEs and genes that do not share an expression profile.

Impact of TE De-repression Dynamics on Virulence

Effectors are frequently among the closest genes to TEs and play a key role in virulence. To dissect the role of TE de-repression in virulence, we first analyzed all 1,381 predicted effector orthologs across the four genomes (Plissonneau et al. 2018). We found that 320 effector orthologs were within 1 kb of a TE and 447 were within 2 kb of a TE. Effector genes with a TE insertion within 1 kb showed higher expression at the peak of symptom development on the host (12–14 dpi) compared with other effectors (fig. 7 and supplementary fig. S13, Supplementary Material online). This suggests that effector genes sharing genomic compartments with TEs benefit from the epigenetic landscape to optimize upregulation during the critical period of infection.

Given the synchronicity in the expression of effectors and de-repression of TEs over the course of a plant infection, we investigated potential causal links between TE de-repression and virulence. Mapping populations generated for two pairs of the four strains analyzed here revealed a major effect locus in each of the strain pairings (Zhong et al. 2017; Stewart et al. 2018). In progeny populations of the cross 3D1×3D7, the locus on chromosome 7 encoding the effector Avr3D1 explains nearly all variation in virulence on the wheat cultivar Runal (Meile et al. 2018). Analysis of deletion and ectopic insertion mutants revealed that the strain 3D7 carries 12 amino acid substitutions and one indel in Avr3D1 and at least a subset of these mutations are critical for successfully avoiding recognition and infecting the host (Meile et al. 2018).

Interestingly, Avr3D1 shows regulatory variation, which may also contribute to differences in virulence. Indeed, Avr3D1 shows much stronger but delayed expression in the avirulent strain 3D1 compared with earlier and lower expression in the virulent strain 3D7 (fig. 8B).

In Z. tritici, heterochromatin remodeling plays a major role in effector expression during the switch to necrotrophy (i.e., the appearance of lesions) (Soyer et al. 2019). The necrotrophic infection period corresponds to the peak expression of Avr3D1 in both 3D1 and 3D7 (fig. 8B). Hence, we investigated evidence for epigenetic remodeling of the locus driven by TEs. Avr3D1 is located at the boundary of a gene-rich region in the avirulent strain 3D1 (fig. 8A). We used uniquely mapped RNAseq reads to assess expression variation at the level of individual TE copies. The closest TE to Avr3D1 in 3D1 is the TIR-Mutator element 2 at 12.3 kb. This TIR-Mutator copy next to Avr3D1 shows expression nearly exclusively at 12 dpi, whereas other copies in the genome were mostly expressed under different conditions and infection stages (fig. 8A and supplementary fig. S14A, Supplementary Material online). The unknown TE element 8 has three copies close to Avr3D1 showing similar expression profiles (fig. 8A and supplementary fig. S14B, C, and E, Supplementary Material online). The second copy is silenced at 12 dpi but is most expressed at 14 dpi. This is in contrast to the other copies outside of the locus showing the opposite expression profile across conditions. Hence, nearby TEs show expression profiles matching the Avr3D1 expression in the 3D1 strain across infection stages.
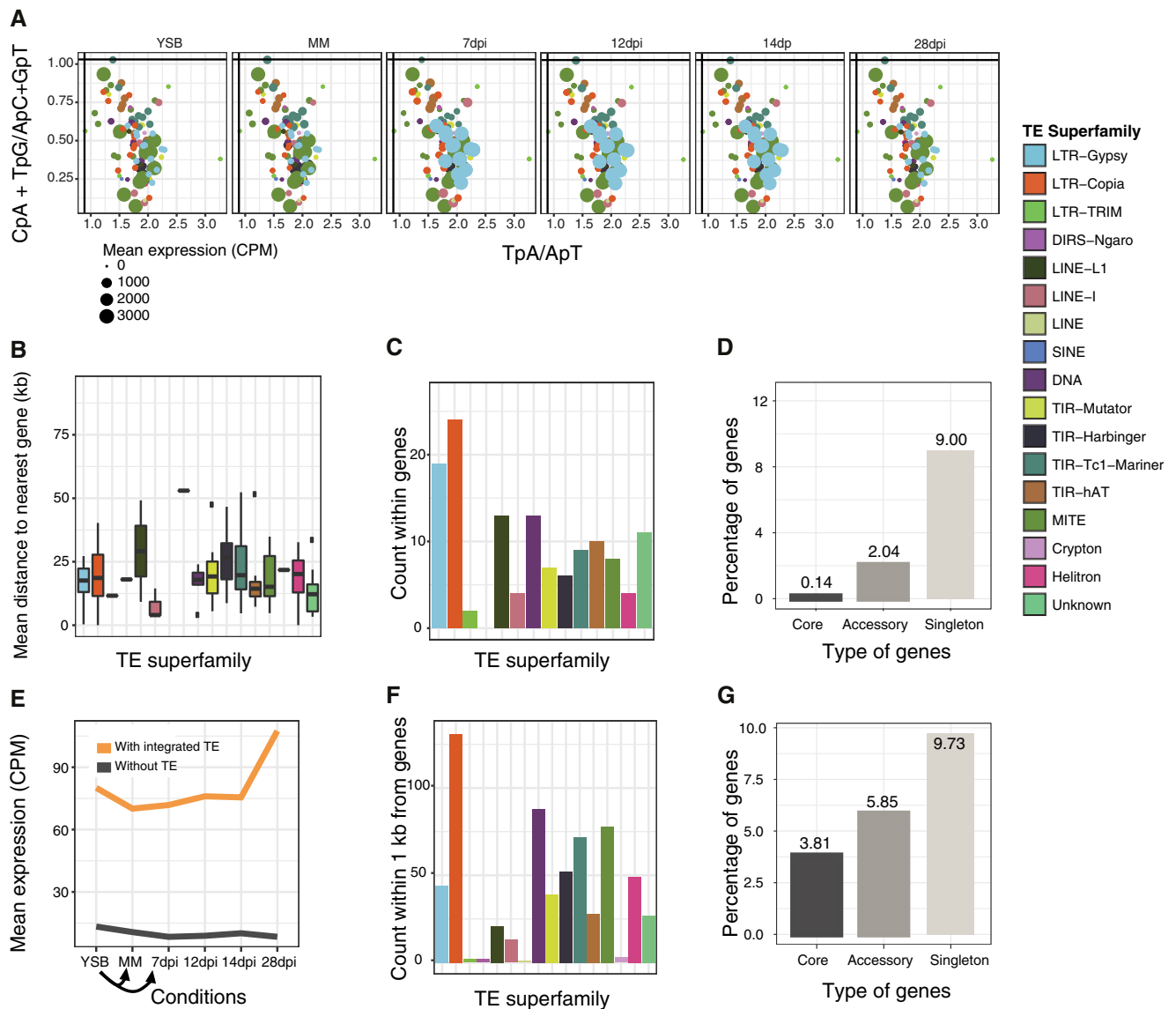
FIG. 6. Genomic defenses and TE expression. (*A*) RIP indices for each TE family and mean expression of the family under all stress conditions for strain 3D1. Vertical and horizontal lines represent commonly used thresholds to detect RIP (Hane and Oliver 2008). Colors indicate the superfamily and size the expression at the family level in CPM. (*B*) The mean interval of TE superfamilies to the nearest gene. (*C*) TE superfamilies within genes in 3D1. (*D*) Gene categories with inserted TEs in 3D1. The percentages are given as the number of genes of that category (core accessory or strain specific) within genes as a fraction of the total number of genes in a category. (*E*) Expression of genes with or without inserted TEs. (*F*) TE superfamilies within 1 kb of the closest gene in strain 3D1. (*G*) Gene categories within 1 kb of TEs. The percentages are given as the number of genes of that category (core, accessory or strain specific) as a fraction of the total number of genes in a category. MM, nutrient poor media; YSB, nutrient rich media.

Next, we analyzed how the epigenetic landscape of TEs evolved in the strain 3D7. This strain gained virulence on the cultivar Runal and the effector is expressed earlier during infection (7–12 dpi; fig. 8B). The *Avr3D1* locus experienced a drastic reconfiguration with the insertion of two large TE clusters (Meile et al. 2018). The closest TE, a copy of a *Crypton* element 1, as well as TE copies in the same cluster were only expressed at 14 dpi but silenced during the peak of symptom developments of the strain 3D7 (fig. 8A and supplementary fig. S15, Supplementary Material online). Other copies of TEs present near *Avr3D1* showed variable de-repression patterns peaking either under nutrient starvation (MM) or during the late infection stage (28 dpi). These atypical de-repression

profiles are characterized by a resilience to de-repression during early stages of host infection. Interestingly, the large TE cluster inserted in 3D7 impacted a boundary region of euchromatin and facultative heterochromatin in the reference genome of IPO323 (fig. 8C). The presence of large TE clusters leads to obligate heterochromatin and strong silencing (Schotanus et al. 2015). This would be consistent with the TE silencing observed near *Avr3D1* in the 3D7 genome. The *Avr3D1* locus is furthermore located at a major epigenetic boundary region of chromosome 7 splitting off a chromosomal arm with nearly uniform H3K27m3 facultative heterochromatin (fig. 8C) (Schotanus et al. 2015). Taken together, our analyses show that the reduced expression of *Avr3D1* in
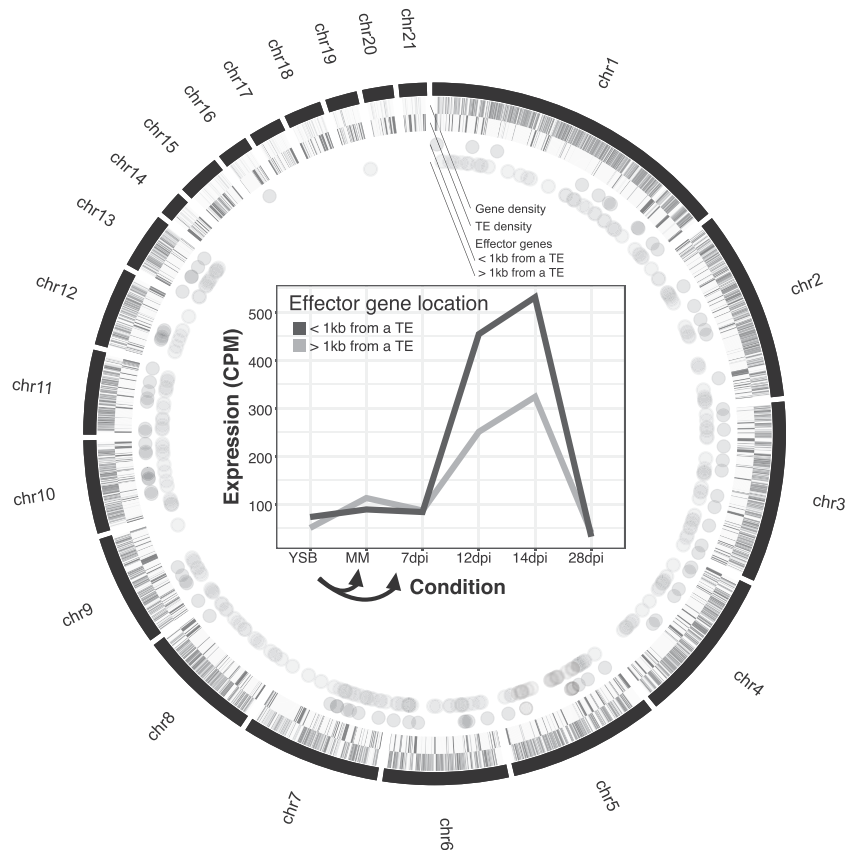
Fig. 7. Effector gene expression according to the presence or absence of nearby TEs. Circular representation of the 3D1 genome with gene and TE density in 10-kb windows, as well as the position of predicted effectors. MM, nutrient poor media; YSB, nutrient rich media.

the virulent strain 3D7 is most consistently explained by the presence of strongly silenced TEs, which do not respond to stress triggers caused by host infection.

Discussion

TEs are major drivers of genome evolution due to their transpositional activity. Repression of TEs is largely governed through epigenetic control and is, hence, susceptible to external stress. Using transcriptome profiling, we show that two distinct stress conditions induce the expression of distinct sets of TEs. By replicating the analyses across four genetic backgrounds, we show that the major expression dynamics of TEs are conserved. However, some of the most highly expressed TEs including MITE and LTR-*Gypsy* elements showed highly distinct de-repression across stress conditions. The genomic context of TEs was a major predictor of de-repression dynamics during stress. Consistent with TE de-repression being governed by epigenetic effects, we found that gene expression profiles under stress varied significantly depending on the proximity to the closest TEs. The evolution of virulence was most likely due to TE-driven epigenetic reconfigurations impacting expression profiles across a major effector locus encoding Avr3D1.

Stress-Dependent TE De-repression Dynamics

The completely assembled genomes of *Z. tritici* display substantial variability in chromosome-level TE content despite highly similar overall repetitive element proportions. The TE content variation is striking given the fact that all four strains were collected from nearby wheat fields, interfertile and from populations with a rapid decay in linkage disequilibrium (Croll et al. 2015). LTR-*Gypsy* were the most abundant elements consistent with their abundance in many other fungal genomes (Muszewska et al. 2011). Members of the LTR-*Gypsy* superfamily in conjunction with an MITE showed among the strongest de-repression under stress. MITEs and LTR-retrotransposons are also most frequently associated with stress responsiveness in other organisms (Yasuda et al. 2013; Negi et al. 2016). However, the impact of stress on TE expression is highly variable among TE families, copies, and species. Some TEs are expressed and potentially mobilized in response to stress, whereas other TEs are suppressed after an initial stress-induced activation, and some TEs are downregulated in response to stress (Horváth et al. 2017).

Nutrient starvation and host infection constitute the major stress factors in the life cycle of filamentous plant pathogens (Ferreira et al. 2006; Hernández-Chávez et al. 2017). We exposed *Z. tritici* to two stress conditions. Growth in a carbon source depleted culture medium (MM) exposed the fungus to nutrient starvation. Early infection stages induce stress due to host immune responses targeted at the pathogen and imposes growth under limited nutrient conditions. CAZymes showed highly distinct profiles depending on the stress condition. Hence, starvation and infection stress have distinct impacts on gene expression consistent with the
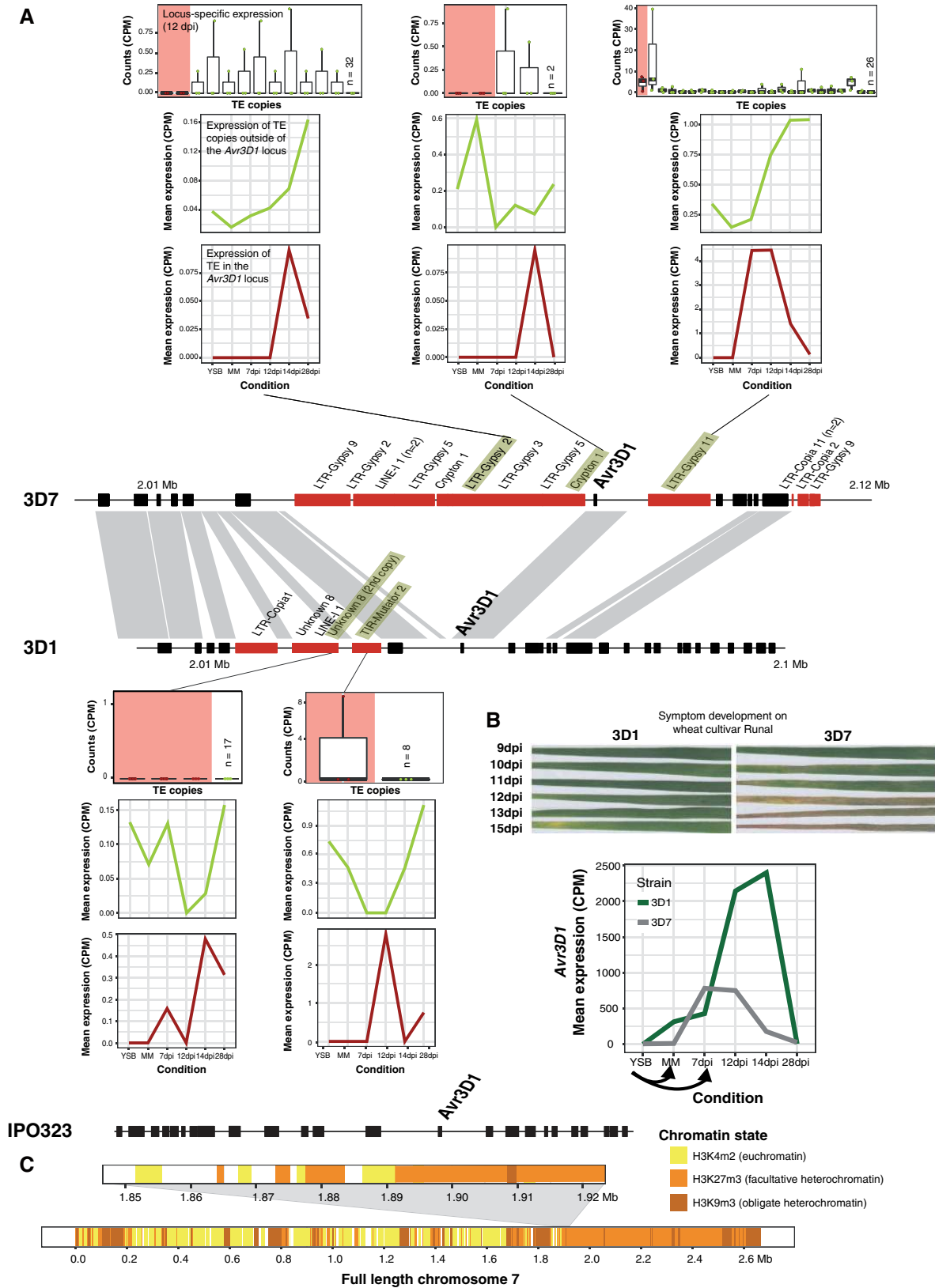
FIG. 8. TE de-repression of individual TEs inserted in proximity to the effector gene *Avr3D1*. (*A*) Synteny plots of the chromosomal regions encoding Avr3D1 in strains 3D7, 3D1, and IPO323. Genes are shown in black and inserted TEs in red. Expression levels of five TEs in close proximity of *Avr3D1* are shown in more detail. The top plot shows expression levels at 12 days post-infection (dpi) of all identified copies across the genome using uniquely mapped reads (expression levels of some copies were summarized). Variation is expressed by showing uniquely mapped reads from each individual replicate. The TE copy highlighted in red corresponds to the copy inserted nearby *Avr3D1*. The middle plot shows averaged expression

biological context of the stress (Palma-Guerrero et al. 2016). The majority of TE families showed some degree of de-repression in at least one of the stress conditions. Elements in the LTR-*Gypsy* superfamily were upregulated during early infection, which corresponds to the most stressful period on the host (Rudd et al. 2015; Palma-Guerrero et al. 2016). Infection stress first causes the upregulation of effector genes and later cell-wall degrading enzymes (Skibbe et al. 2010; Wang et al. 2011; Kleemann et al. 2012; Hacquard et al. 2013; Soyer et al. 2014; Palma-Guerrero et al. 2016). Effector gene expression is known to be epigenetically regulated in plant pathogens and timed to maximize exploitation of the host (Qutob et al. 2013; Schotanus et al. 2015; Sánchez-Vallet et al. 2018; Soyer et al. 2019). We found that a different set of TEs showed the highest expression under starvation stress including an MITE, which was the most strongly expressed TE in the genomes. The regulatory framework governing stress responses is largely unknown in *Z. tritici*, but distinct epigenetic regulation in response to stress is likely playing a key role (Schotanus et al. 2015; Soyer et al. 2019).

TE and Gene Co-expression Dependent on the Genomic Environment

Genes and TEs in close physical proximity likely undergo joint epigenetic regulation in response to stress. We found that genes close to TEs were upregulated during early infection consistent with the de-repression observed for TEs. LTR-*Copia* elements were the most frequently found TEs close to genes, and one LTR-*Copia* family showed upregulation during early infection. In contrast, genes far from TEs were upregulated toward the end of the infection cycle, which is after the transition to a less stressful saprophytic lifestyle (Palma-Guerrero et al. 2016). Interestingly, we found no association of gene-to-TE distance with expression under nutrient starvation stress. This distinction may be due to the fact that epigenetic control of TEs is less pronounced under nutrient starvation stress. To understand TE de-repression dynamics as a function of the genomic environment, we also analyzed mean distances of TE families to the closest genes. Due to the repetitive nature of TEs, most transcriptome-derived short sequences cannot reliably be assigned to a single TE copy. Hence, our distance analyses were performed using summary statistics per TE family and not per individual TE copy. Copies of the most highly expressed TE, an MITE-Undine, are 17.6–33.8 kb away from genes across all genetic backgrounds. This activation could still be affecting the expression of genes as was shown for the Hopscotch TE in maize. This TE influences the expression of the TB1 locus at a distance of ~60 kb (Studer et al. 2011).

Based on our co-expression clustering analyses, we found that TEs were not physically closer to coexpressed genes than other genes, suggesting that coregulation is occurring in *trans* rather than in *cis*. Alternatively, this may reflect the epigenetic landscape of the genome with a multitude of distal chromosomal regions showing concerted de-repression dynamics. Interestingly, in other fungi such as *Coccidioides* (Kirkland et al. 2018) and *Pleurotus* (Borgognone et al. 2018) species, genes within 1 kb of some TE families were more repressed than genes overall and these genes were enriched for kinase function in *Coccidioides* species. In other organisms, the influence of a TE on nearby genes is largely determined by the chromatin state of the TE (Saze and Kakutani 2007; Martin et al. 2009; Zeng and Cheng 2014; Lei et al. 2015; Williams et al. 2015; Hirsch and Springer 2017). This is most evident for stress-responsive genes that carry TE insertions in the promoter sequences leading to upregulation upon TE demethylation (Le et al. 2014). Whether TE silencing through chromatin modification can spread to adjacent genes is not well understood (Sienski et al. 2012; Le Thomas et al. 2013; Lee 2015). TE stress responsiveness can be governed by epigenetic de-repression (Slotkin and Martienssen 2007) or the loss of a repressive mechanism under stress (Van Meter et al. 2014). If all TEs showed a correlated response to stress, this would suggest that activation is mostly due to epigenetic effects alone. However, different TE families show different stress responsiveness according to the stress condition and the host genotype, suggesting distinct epigenetic environments between the strains.

The Role of the Genetic Background in TE Expression Dynamics

The set of four completely assembled con-specific genomes enabled us to analyze de-repression dynamics of the same TEs across different genetic backgrounds. We found that TE family expression differed between the strains indicating that the genetic background plays a role in the ability of TEs to respond to stress. Several LTR-*Gypsy* elements were upregulated early during infection in one genetic background but not in all. TE families in close proximity to genes were upregulated during early infection in strains 3D1 and 1E4, whereas families with the longest average distance to genes were upregulated during infection in strain 3D7. Our evidence for TE family expression by genetic background interactions suggests high degrees of polymorphism for TE control within the species. In *A. thaliana*, TE responsiveness to cold stress was found to differ among ecotypes and this was largely explained by differences in the genomic locations of specific TEs (Barah et al. 2013). Such variation in the ability to control TE expression provides selectable genetic variation for the host genome to evolve more efficient control mechanisms.

Fig. 8. Continued

levels of all TE copies outside of the *Avr3D1* locus. The bottom plot shows the expression levels of the TE copy found nearby *Avr3D1*. (*B*) Disease progress and symptom development by 3D1 and 3D7 infecting the wheat cultivar Runal (Meile et al., 2018). The expression variation of *Avr3D1* is shown below in wheat cultivar Drifter. (*C*) Histone methylation marks assessed for the reference genome IPO323 (Schotanus et al. 2015). Both the region of *Avr3D1* as well as the entire chromosome 7 are shown. MM, nutrient poor media; YSB, nutrient rich media.

Stress De-repression of TEs and the Evolution of TE Control Mechanisms

Derepressed TEs are mutagenic (Le Rouzic and Capy 2005) and can lead to genome expansions (Lonnig and Saedler 2002). Hence, host genomes evolved to suppress TE proliferation. Stress responsiveness of TE families is indicative of the ability by the host to control proliferation. The MITE with the highest expression is consistently expressed in all conditions, suggesting that the host genome has not yet evolved effective control mechanisms. RIP is a genomic defense mechanism that hypermutates duplicated DNA sequences in fungi and counteracts TE proliferation (Selker 2002). We found that TE families with signatures of RIP were still responsive to stress. In particular, the highly responsive MITE and LTR-*Gypsy* elements under starvation and infection stress, respectively, display strong signatures of RIP. This suggests that point mutations introduced by RIP may well introduce loss-of-function mutations and disable, for example, transposase functions. However, RIP in *Z. tritici* seems ineffective at preventing TE de-repression under stress.

Pathogens of plants are exposed to unique stress conditions upon entering their host. The challenges mounted by the plant immune system are designed to effectively contain a pathogen's deployment of its infection program. Specialized pathogens evolved to time the expression of pathogenicity factors with the onset of stress by localizing the underlying genes in epigenetically silenced chromosomal regions (Sánchez-Vallet et al. 2018). We show here that the colocalization of epigenetically silenced TEs and effector genes can underlie major adaptations to successfully circumvent detection by the host. Although the localization of pathogenicity factors in epigenetically silenced regions is most likely adaptive for the pathogen, the localization of TEs in the same compartment is likely only adaptive in absence of stress. Hence, the colocalization of pathogenicity factors and TEs creates a complex selection regime on the pathogen. Selection for more effective TE control under infection stress may actually be deleterious for the coordinated gene expression during infection. We identified unexpected complexity in both the genomic localization of TEs across genetic backgrounds and in the TEs response to stress. This suggests that there is standing variation for the ability to control TEs within the species. Hence, host genomes and TEs may be engaged in rapid coevolutionary arms races to maintain effective control and escape repression, respectively.

Materials and Methods

Strains and Growth Conditions

Strains 1A5, 1E4, 3D1, and 3D7 were isolated from two fields in Switzerland in 1999, and they have been phenotypically and genotypically characterized (Zhan et al. 2005; Croll et al. 2013). These strains were used in previous studies for quantitative loci mapping (Lendenmann et al. 2014, 2016; Stewart and McDonald 2014; Stewart et al. 2018). The genomes of all four strains have been sequenced and assembled into complete chromosomes using high-coverage PacBio sequencing (Plissonneau et al. 2016, 2018). High-density genetic maps (Lendenmann et al. 2014; Croll et al. 2015) were used to validate each assembly.

Gene and Repetitive Element Annotation

We used pangenome gene annotation generated by Plissonneau et al. (2018). Genes were predicted by using splicing evidence from the in planta RNA-seq data from the same time points and strains as described above. Repetitive elements were annotated in all four genomes using RepeatMasker 4.0.5 (Smith, 1996) and a repeat element library for the reference genome (IPO323) produced by Grandaubert et al. (2015). This library was created using the REPET pipeline (Flutre et al. 2011). Repeat families in each species were clustered with BLASTClust from the NCBI-BLAST package (Altschul et al. 1990) and aligned with MAFFT (Katoh and Standley 2013) to create new consensus sequences. This process was repeated with lower identity percentages (from 100% to 75% identity) and lower coverage (from 100% to 30%) until sequences did not form new clusters anymore. The repetitive sequences were classified with the TEClassifier.py script from REPET using TBlastX and BlastX against the Giri Repbase Update database (Jurka et al. 2005) and by the identification of characteristic TE features such as LTRs. The sequences were also translated into the six reading frames in order to identify protein domains in the conserved domain database (Marchler-Bauer et al. 2011) using RPS-BLAST. Identified repetitive sequences were finally named according to the three-letter nomenclature defined by Wicker et al. (2007). The single TE library enables the comparison of TEs between the four strains as all the elements have exactly the same naming. RepeatMasker was used with the following parameters: pa 2, -s, and –a for using two parallel processors, in slow mode for increased sensitivity and generating an alignment output file. Additional elements were identified using MITEtracker with default parameters (Crescente et al. 2018).

RNA Extractions, Library Preparation, and Sequencing

Seedlings of the wheat cultivar "Drifter" were infected with the four strains 3D1, 3D7, 1E4, and 1A5, on the same day and in the same greenhouse chamber (Palma-Guerrero et al. 2016, 2017). Total RNA was extracted from inoculated second leaves at time points 7, 12, 14, and 28 dpi using a TRIzol (Invitrogen) extraction protocol (Palma-Guerrero et al. 2017). The time points were selected to include asymptomatic (biotrophic), necrotrophic, and the saprophytic stages of infection. In addition, a TRIzol RNA extraction was performed for all four strains in a nutrient limited, defined salts medium without sucrose (Minimal Medium—MM pH 5.8) and a nutrient-rich YSB media (10 g/l sucrose and 10 g/l yeast extract, pH 6.8) (Vogel 1956; Francisco et al. 2018). Cells were recovered in YSB medium and then transferred to either YSB or MM, incubated for 4 days at 18 °C, prior to harvest for RNA extraction. For the infection experiments, cells were harvested from three leaf samples from each time point for the in planta samples and three in vitro samples for each condition. Samples with the highest RNA quality as determined with a Bioanalyzer 2100 (Agilent) were selected as biological

replicates for each time point for library preparation and sequencing. RNA quantity was assessed with a Qubit fluorometer (Life Technologies), and libraries were prepared using the TruSeq stranded mRNA sample prep kit (Illumina Inc.) according to the provided protocol. Total RNA samples were ribosome depleted by using PolyA selection and reverse-transcribed into double-stranded cDNA. Actinomycin was added during the first-strand synthesis. The cDNA was then fragmented, end-paired and an A-tail was added before the ligation of the TruSeq adapters. A selective enrichment for fragments with TruSeq adapters on each end was performed by polymerase chain reaction. The quality and quantity of the enriched libraries were verified with a Qubit (1.0) fluorometer and a Tapestation (Agilent). Paired-end libraries were sequenced on an Illumina HiSeq 2500 with read lengths of 2 × 125 bp (Illumina Inc.) for the in planta samples and with read lengths of 4 × 100 bp for the in vitro conditions.

Transcription Mapping and Quantification

Raw sequencing reads were quality-trimmed and filtered for adapter contamination and low-quality reads using Trimmomatic 0.36 (Bolger et al. 2014) using the following parameters: ILLUMINACLIP: TruSeq3-PE.fa: 2: 30: 10 LEADING: 10 TRAILING: 10 SLIDINGWINDOW: 5: 10 MINLEN: 50. Trimmed and filtered reads were mapped to the reference genome sequence of the specific strain (Plissonneau et al. 2018) using STAR 2.6.0 (Dobin and Gingeras 2016) allowing multiple mapped reads with the following settings: –outFilterMultimapNmax 100 –winAnchorMultimapNmax 200 –outSAMtype BAM Unsorted –outFilterMismatchNmax 3, according to the recommended parameters for TE analyses (Jin et al. 2015; Jin and Hammell 2018). We performed a saturation analysis to determine the cut-off to be used for the optimal number of reported alignments of a specific read, where increasing the threshold did not increase the number of mapped reads significantly as recommended (Jin and Hammell 2018) (supplementary fig. S1 and table S1, Supplementary Material online). The resulting unsorted bamfiles were sorted by read name with SAMtools 1.9 and the expression levels of TEs and genes were quantified using TEtranscripts 2.0.3 (Jin et al. 2015) with the following parameters: –stranded no –mode multi -p 0.05 -i 10. TEtranscripts counts uniquely and multiple-mapped reads that align to genes and TE regions to determine TE- and gene-level transcript abundance. The software assumes that transcribed TEs will have reads mapping along the entire length of the element (Jin and Hammell 2018). Elements with reads mapping to only a fraction of the length were assumed to be nontranscribed as these subregions may not be unique enough in the genome compared with, for example, other TEs.

TE and gene read counts were normalized between replicates and time points for the in planta and in vitro samples using the R/Bioconductor package EdgeR 3.8 (Robinson and Smyth 2007; Robinson and Oshlack 2010; Robinson et al. 2010). Genes and TEs without at least one read in all the samples were excluded for the normalization step (Anders

et al. 2013) and were assumed for the rest of the analyses to have zero expression. Library sizes were normalized with the TMM method (Robinson and Oshlack 2010). CPM (counts per million) were generated with the EdgeR CPM function using TMM-normalized libraries.

Locus-Specific TE Expression between 3D1 and 3D7

We analyzed transcriptomic reads for unique mapping (i.e., to a single genomic region) and extracted reads with the samtools view -q 255 (the flag assigned by the STAR aligner). Reads were quantified with htseq_count 0.8.0 and normalized as described above to generate CPM for each copy of a TE with locus-specific expression information. The genomic region encoding the effector Avr3D1 was compared between the genomes of 3D7, 3D1, and IPO323 using pairwise BlastN on repeat-masked genomes. Hits were filtered for a minimum identity of 95%, e-values reported as effectively 0. Synteny blocks were visualized using the R package genoPlotR (Guy et al. 2010).

Genomic Localization of TEs and Co-expression Analyses

In order to investigate the association of the genomic environment with TE expression, we identified the nearest gene to each TE using bedtools 2.27 command *closest* with the option to report only the closest TE to each gene and to allow overlaps to include genes that have been disrupted by intragenic TEs (Quinlan and Hall 2010). Co-expression clusters were computed using the Short Time-Series Expression Miner (STEM) software 1.3.11, designed to analyze time series with 3–8 time points (Ernst et al. 2005; Ernst and Bar-Joseph 2006). STEM software uses a nonparametric clustering method to assign genes to predefined expression profiles. It considers expression profiles to be significant if the number of genes assigned to a cluster departs from random. We used all three individual replicates per condition and isolate (option: repeat data) and transformed all data using log normalization. The analysis identified a total of 20 co-expression profiles, namely 8–9–13–15–16–17–18–19–20–21–27–28–29–31–32–33–35–36–37, and 39. The statistical significance of the number of genes assigned to each profile was computed by applying a Bonferroni correction with $\alpha = 0.05$. The biological relevance of co-expression profiles was assessed by GO term enrichment analysis (Ernst et al. 2005; Ernst and Bar-Joseph 2006). STEM software implements a GO term enrichment method that uses the hypergeometric distribution based on the number of genes assigned to the co-expression profile, the number of genes assigned to the GO category, and the number of unique genes in the experiment. Enrichment significance was corrected by using randomization tests.

RIP Analysis

We identified RIP by aligning each copy of a given TE with the consensus sequence using MAFFT 7.407 (Katoh et al. 2002; Katoh and Standley 2013). The consensus sequence could be more affected by RIP than individual TE copies in the genome because mutations occurring in a given sequence are likely to be removed by the "base-pair majority rule" used to build the

consensus. In this case, the copy with the highest GC content (i.e., the least affected by RIP) is used as the RIPCAL 1.0 input (Hane and Oliver 2008). All TE families (individual TE copies and the consensus) were aligned and processed by RIPCAL using default parameters (Hane and Oliver 2008). RIPCAL output provides the number of transition and transversions, single mutations, and dinucleotide targets used in all possible transition mutations for each genomic TE copy. The RIPCAL output can be used to determine whether individual TE copies are "RIPped" based on two indices: (CpA+TpG)/(ApC+GpT) indicating a decrease in RIP targets and TpA/ApT indicating an increase in RIP products. We used the default criteria where a (CpA+TpG)/(ApC+GpT) ratio of below 1.03 is indicative of RIP and a TpA/ApT of higher than 0.89 is indicative of RIP (Hane and Oliver 2008). In general, TE families with a lower (CpA+TpG)/(ApC+GpT) value and a higher TpA/ApT are more affected by RIP (Hane and Oliver 2008). We excluded unknown elements from this analysis. R (R Core Team 2017) was used to generate graphics from RIPCAL outputs. These outputs were parsed to search for RIP signatures in TE copies and the dinucleotide targets used in the transition type mutations that are usually associated with RIP.

Supplementary Material

Supplementary data are available at *Molecular Biology and Evolution* online.

Acknowledgments

Author Contributions

S.F., C.P., and D.C.: conceived the study; S.F., T.B., U.O., and C.P.: performed analyses; C.S.F.: contributed data set; S.F. and D.C.: wrote the manuscript.

References

Altschul SF, Gish W, Miller W, Myers EW, Lipman DJ. 1990. Basic local alignment search tool. *J Mol Biol.* 215(3):403–410.

Anders S, McCarthy DJ, Chen Y, Okoniewski M, Smyth GK, Huber W, Robinson MD. 2013. Count-based differential expression analysis of RNA sequencing data using R and Bioconductor. *Nat Protoc.* 8(9):1765–1786.

Barah P, Jayavelu ND, Rasmussen S, Nielsen HB, Mundy J, Bones AM. 2013. Genome-scale cold stress response regulatory networks in ten *Arabidopsis thaliana* ecotypes. *BMC Genomics* 14:722.

Bolger AM, Lohse M, Usadel B. 2014. Trimmomatic: a flexible trimmer for Illumina sequence data. *Bioinformatics* 30(15):2114–2120.

Borgognone A, Castanera R, Morselli M, López-Varas L, Rubbi L, Pisabarro AG, Pellegrini M, Ramírez L. 2018. Transposon-associated epigenetic silencing during *Pleurotus ostreatus* life cycle. *DNA Res.* 25:451–464.

Bucher E, Reinders J, Mirouze M. 2012. Epigenetic control of transposon transcription and mobility in *Arabidopsis*. *Curr Opin Plant Biol.* 15(5):503–510.

Bundo M, Toyoshima M, Okada Y, Akamatsu W, Ueda J, Nemoto-Miyauchi T, Sunaga F, Toritsuka M, Ikawa D, Kakita A. 2014. Increased l1 retrotransposition in the neuronal genome in schizophrenia. *Neuron* 81(2):306–313.

Capy P, Gasperi G, Biémont C, Bazin C. 2000. Stress and transposable elements: co-evolution or useful parasites? *Heredity* 85(2):101–106.

Casacuberta E, González J. 2013. The impact of transposable elements in environmental adaptation. *Mol Ecol.* 22(6):1503–1517.

Cavrak VV, Lettner N, Jamge S, Kosarewicz A, Bayer LM, Scheid OM. 2014. How a retrotransposon exploits the plant's heat stress response for its activation. *PLoS Genet.* 10(1):e1004115.

Chujo T, Scott B. 2014. Histone H3K9 and H3K27 methylation regulates fungal alkaloid biosynthesis in a fungal endophyte-plant symbiosis. *Mol Microbiol.* 92(2):413–434.

Chuong EB, Elde NC, Feschotte C. 2017. Regulatory activities of transposable elements: from conflicts to benefits. *Nat Rev Genet.* 18(2):71–86.

Connolly LR, Smith KM, Freitag M. 2013. The *Fusarium graminearum* histone H3 K27 methyltransferase KMT6 regulates development and expression of secondary metabolite gene clusters. *PLoS Genet.* 9(10):e1003916.

Cowley M, Oakey RJ. 2013. Transposable elements re-wire and fine-tune the transcriptome. *PLoS Genet.* 9(1):e1003234.

Crescente JM, Zavallo D, Helguera M, Vanzetti LS. 2018. MITE Tracker: an accurate approach to identify miniature inverted-repeat transposable elements in large genomes. *BMC Bioinformatics* 19(1):348.

Croll D, Lendenmann MH, Stewart E, McDonald BA. 2015. The impact of recombination hotspots on genome evolution of a fungal plant pathogen. *Genetics* 201(3):1213–1228.

Croll D, McDonald BA. 2012. The accessory genome as a cradle for adaptive evolution in pathogens. *PLoS Pathog.* 8(4):e1002608.

Croll D, Zala M, McDonald BA. 2013. Breakage-fusion-bridge cycles and large insertions contribute to the rapid evolution of accessory chromosomes in a fungal pathogen. *PLoS Genet.* 9(6):e1003567.

Derridj S. 1996. Nutrients on the leaf surface. In: Morris CE, Nicot PC, Nguyen-The C, editors. Aerial plant surface microbiology. Boston: Springer US. p. 25–42. Available from: https://doi.org/10.1007/978-0-585-34164-4_2 (last accessed January 22, 2019).

Dillon N. 2004. Heterochromatin structure and function. *Biol Cell.* 96(8):631–637.

Dobin A, Gingeras TR. 2016. Optimizing RNA-seq mapping with STAR. *Methods Mol Biol.* 1415:245–262.

Doolittle WF, Sapienza C. 1980. Selfish genes, the phenotype paradigm and genome evolution. *Nature* 284(5757):601–603.

Dubin MJ, Mittelsten Scheid O, Becker C. 2018. Transposons: a blessing curse. *Curr Opin Plant Biol.* 42:23–29.

Ernst J, Bar-Joseph Z. 2006. STEM: a tool for the analysis of short time series gene expression data. *BMC Bioinformatics* 7:191.

Ernst J, Nau GJ, Bar-Joseph Z. 2005. Clustering short time series gene expression data. *Bioinformatics* 21(Suppl 1):i159–168.

Ferreira RB, Monteiro S, Freitas R, Santos CN, Chen Z, Batista LM, Duarte J, Borges A, Teixeira AR. 2006. Fungal pathogens: the battle for plant infection. *Crit Rev Plant Sci.* 25(6):505–524.

Flutre T, Duprat E, Feuillet C, Quesneville H. 2011. Considering transposable element diversification in *de novo* annotation approaches. *PLoS One* 6(1):e16526.

Fones H, Gurr S. 2015. The impact of *Septoria tritici* Blotch disease on wheat: an EU perspective. *Fungal Genet Biol.* 79:3–7.

Fouché S, Plissonneau C, Croll D. 2018. The birth and death of effectors in rapidly evolving filamentous pathogen genomes. *Curr Opin Microbiol.* 46:34–42.

Francisco CS, Ma X, Zwyssig MM, McDonald BA, Palma-Guerrero J. 2019. Morphological changes in response to environmental stresses in the fungal plant pathogen *Zymoseptoria tritici*. Sci. Rep. 9:1–18.

Galindo-González L, Mhiri C, Deyholos MK, Grandbastien M-A. 2017. LTR-retrotransposons in plants: engines of evolution. *Gene* 626:14–25.

Goodwin SB, Ben M'Barek S, Dhillon B, Wittenberg AHJ, Crane CF, Hane JK, Foster AJ, Van der Lee TAJ, Grimwood J, Aerts A, et al. 2011. Finished genome of the fungal wheat pathogen *Mycosphaerella graminicola* reveals dispensome structure, chromosome plasticity, and stealth pathogenesis. *PLoS Genet.* 7(6):e1002070.

Grandaubert J, Bhattacharyya A, Stukenbrock EH. 2015. RNA-seq-based gene annotation and comparative genomics of four fungal grass pathogens in the genus *Zymoseptoria* identify novel orphan genes and species-specific invasions of transposable elements. *G3* 5:1323–1333.

Guy L, Roat Kultima J, Andersson S. 2010. genoPlotR: comparative gene and genome visualization in R. *Bioinformatics* 26(18):2334–2335.

Hacquard S, Kracher B, Maekawa T, Vernaldi S, Schulze-Lefert P, Themaat E. V. 2013. Mosaic genome structure of the barley powdery mildew pathogen and conservation of transcriptional programs in divergent hosts. *Proc Natl Acad Sci U S A.* 110(24):E2219–E2228.

Hane JK, Oliver RP. 2008. RIPCAL: a tool for alignment-based analysis of repeat-induced point mutations in fungal genomic sequences. *BMC Bioinformatics* 9:478.

Hartmann FE, Sánchez-Vallet A, McDonald BA, Croll D. 2017. A fungal wheat pathogen evolved host specialization by extensive chromosomal rearrangements. *ISME J.* 11(5):1189–1204.

Haueisen J, Möller M, Eschenbrenner CJ, Grandaubert J, Seybold H, Adamiak H, Stukenbrock EH. 2019. Highly flexible infection programs in a specialized wheat pathogen. *Ecol Evol.* 9(1):275–294.

Hernández-Chávez MJ, Pérez-García LA, Niño-Vega GA, Mora-Montes HM. 2017. Fungal strategies to evade the host immune recognition. *J. Fungi* 3:51.

Hirsch CD, Springer NM. 2017. Transposable element influences on gene expression in plants. *Biochim Biophys Acta Gene Regul Mech.* 1860(1):157–165.

Horváth V, Merenciano M, González J. 2017. Revisiting the relationship between transposable elements and the eukaryotic stress response. *Trends Genet.* 33(11):832–841.

Huang J, Wang Y, Liu W, Shen X, Fan Q, Jian S, Tang T. 2017. *EARE-1*, a transcriptionally active Ty1/Copia-like retrotransposon has colonized the genome of *Excoecaria agallocha* through horizontal transfer. *Front Plant Sci.* 8:45.

Hummel B, Hansen EC, Yoveva A, Aprile-Garcia F, Hussong R, Sawarkar R. 2017. The evolutionary capacitor HSP90 buffers the regulatory effects of mammalian endogenous retroviruses. *Nat Struct Mol Biol.* 24(3):234–242.

Ito H, Gaubert H, Bucher E, Mirouze M, Vaillant I, Paszkowski J. 2011. An siRNA pathway prevents transgenerational retrotransposition in plants subjected to stress. *Nature* 472(7341):115–119.

Jin Y, Hammell M. 2018. Analysis of RNA-seq data using TEtranscripts. In: Wang Y, Sun M, editors. Transcriptome data analysis: methods and protocols. Methods in molecular biology. New York: Springer. p. 153–167. Available from: https://doi.org/10.1007/978-1-4939-7710-9_11, last accessed March 20, 2019.

Jin Y, Tam OH, Paniagua E, Hammell M. 2015. TEtranscripts: a package for including transposable elements in differential expression analysis of RNA-seq datasets. *Bioinformatics* 31(22):3593–3599.

Jurka J, Kapitonov VV, Pavlicek A, Klonowski P, Kohany O, Walichiewicz J. 2005. Repbase Update, a database of eukaryotic repetitive elements. *Cytogenet Genome Res.* 110(1–4):462–467.

Katoh K, Misawa K, Kuma K, Miyata T. 2002. MAFFT: a novel method for rapid multiple sequence alignment based on fast Fourier transform. *Nucleic Acids Res.* 30(14):3059–3066.

Katoh K, Standley DM. 2013. MAFFT multiple sequence alignment software version 7: improvements in performance and usability. *Mol Biol Evol.* 30(4):772–780.

Kirkland TN, Muszewska A, Stajich JE. 2018. Analysis of transposable elements in Coccidioides species. *J. Fungi* 4:13.

Kleemann J, Rincon-Rivera LJ, Takahara H, Neumann U, Themaat EV, Does HVD, Hacquard S, Stüber K, Will I, Schmalenbach W, et al. 2012. Sequential delivery of host-induced virulence effectors by appressoria and intracellular hyphae of the phytopathogen *Colletotrichum higginsianum*. *PLoS Pathog.* 8(4):e1002643.

Krishnan P, Meile L, Plissonneau C, Ma X, Hartmann FE, Croll D, McDonald BA, Sánchez-Vallet A. 2018. Transposable element insertions shape gene regulation and melanin production in a fungal pathogen of wheat. *BMC Biol.* 16(1):78.

Lanciano S, Mirouze M. 2018. Transposable elements: all mobile, all different, some stress responsive, some adaptive? *Curr Opin Genet Dev.* 49:106–114.

Le T-N, Schumann U, Smith NA, Tiwari S, Au PCK, Zhu Q-H, Taylor JM, Kazan K, Llewellyn DJ, Zhang R, et al. 2014. DNA demethylases target promoter transposable elements to positively regulate stress responsive genes in Arabidopsis. *Genome Biol.* 15(9):458.

Le Rouzic A, Capy P. 2005. The first steps of transposable elements invasion: parasitic strategy vs. genetic drift. *Genetics* 169(2):1033–1043.

Le Thomas A, Rogers AK, Webster A, Marinov GK, Liao SE, Perkins EM, Hur JK, Aravin AA, Tóth KF. 2013. Piwi induces piRNA-guided transcriptional silencing and establishment of a repressive chromatin state. *Genes Dev.* 27(4):390–399.

Lee Y. 2015. The role of piRNA-mediated epigenetic silencing in the population dynamics of transposable elements in *Drosophila melanogaster*. *PLoS Genet.* 11(6):e1005269.

Lei M, Zhang H, Julian R, Tang K, Xie S, Zhu J-K. 2015. Regulatory link between DNA methylation and active demethylation in *Arabidopsis*. *Proc Natl Acad Sci U S A.* 112(11):3553–3557.

Lendenmann MH, Croll D, Palma-Guerrero J, Stewart EL, McDonald BA. 2016. QTL mapping of temperature sensitivity reveals candidate genes for thermal adaptation and growth morphology in the plant pathogenic fungus *Zymoseptoria tritici*. *Heredity* (Edinb). 116(4):384–394.

Lendenmann MH, Croll D, Stewart EL, McDonald BA. 2014. Quantitative trait locus mapping of melanization in the plant pathogenic fungus *Zymoseptoria tritici*. *G3 (Bethesda).* 4(12):2519–2533.

Lonnig W-E, Saedler H. 2002. Chromosome rearrangements and transposable elements. *Annu Rev Genet.* 36:389–410.

Marchler-Bauer A, Lu S, Anderson JB, Chitsaz F, Derbyshire MK, DeWeese-Scott C, Fong JH, Geer LY, Geer RC, Gonzales NR, et al. 2011. CDD: a Conserved Domain Database for the functional annotation of proteins. *Nucleic Acids Res.* 39(Database issue):D225–229.

Martin A, Troadec C, Boualem A, Rajab M, Fernandez R, Morin H, Pitrat M, Dogimont C, Bendahmane A. 2009. A transposon-induced epigenetic change leads to sex determination in melon. *Nature* 461(7267):1135–1138.

McClintock B. 1950. The origin and behavior of mutable loci in maize. *Proc Natl Acad Sci U S A.* 36(6):344–355.

Meile L, Croll D, Brunner PC, Plissonneau C, Hartmann FE, McDonald BA, Sánchez-Vallet A. 2018. A fungal avirulence factor encoded in a highly plastic genomic region triggers partial resistance to *Septoria tritici* blotch. *New Phytol.* 219(3):1048–1061.

Menees TM, Sandmeyer SB. 1996. Cellular stress inhibits transposition of the yeast retrovirus-like element Ty3 by a ubiquitin-dependent block of virus-like particle formation. *Proc Natl Acad Sci U S A.* 93(11):5629–5634.

Miousse IR, Chalbot M-C, Lumen A, Ferguson A, Kavouras IG, Koturbash I. 2015. Response of transposable elements to environmental stressors. *Mutat Res Rev Mutat Res.* 765:19–39.

Mita P, Boeke JD. 2016. How retrotransposons shape genome regulation. *Curr Opin Genet Dev.* 37:90–100.

Muszewska A, Hoffman-Sommer M, Grynberg M. 2011. LTR retrotransposons in fungi. *PLoS One* 6(12):e29425.

Negi P, Rai AN, Suprasanna P. 2016. Moving through the stressed genome: emerging regulatory roles for transposons in plant stress response. *Front Plant Sci.* 7:1448.

Niederhuth CE, Bewick AJ, Ji L, Alabady MS, Kim KD, Li Q, Rohr NA, Rambani A, Burke JM, Udall JA, et al. 2016. Widespread natural variation of DNA methylation within angiosperms. *Genome Biol.* 17(1):194.

Palma-Guerrero J, Ma X, Torriani SFF, Zala M, Francisco CS, Hartmann FE, Croll D, McDonald BA. 2017. Comparative transcriptome analyses in *Zymoseptoria tritici* reveal significant differences in gene expression among strains during plant infection. *Mol Plant Microbe Interact.* 30(3):231–244.

Palma-Guerrero J, Torriani SFF, Zala M, Carter D, Courbot M, Rudd JJ, McDonald BA, Croll D. 2016. Comparative transcriptomic analyses of *Zymoseptoria tritici* strains show complex lifestyle transitions and intraspecific variability in transcription profiles. *Mol Plant Pathol.* 17(6):845–859.

Plissonneau C, Hartmann FE, Croll D. 2018. Pangenome analyses of the wheat pathogen *Zymoseptoria tritici* reveal the structural basis of a highly plastic eukaryotic genome. *BMC Biol.* 16(1):5.

Plissonneau C, Stürchler A, Croll D. 2016. The evolution of orphan regions in genomes of a fungal pathogen of wheat. *mBio* 7(5):e01231–16.

Quinlan AR, Hall IM. 2010. BEDTools: a flexible suite of utilities for comparing genomic features. *Bioinformatics* 26(6):841–842.

Qutob D, Patrick Chapman B, Gijzen M. 2013. Transgenerational gene silencing causes gain of virulence in a plant pathogen. *Nat Commun.* 4:1349.

R Core Team. 2017. R: a language and environment for statistical computing. Vienna (Austria): R Foundation for Statistical Computing. Available from: https://www.R-project.org/, last accessed April 15, 2019.

Robinson MD, McCarthy DJ, Smyth GK. 2010. edgeR: a Bioconductor package for differential expression analysis of digital gene expression data. *Bioinformatics* 26(1):139–140.

Robinson MD, Oshlack A. 2010. A scaling normalization method for differential expression analysis of RNA-seq data. *Genome Biol.* 11(3):R25.

Robinson MD, Smyth GK. 2007. Small-sample estimation of negative binomial dispersion, with applications to SAGE data. *Biostatistics* 9(2):321–332.

Romero-Soriano V, Guerreiro M. 2016. Expression of the retrotransposon *Helena* reveals a complex pattern of TE deregulation in *Drosophila* hybrids. *PLoS One* 11(1):e0147903.

Rouxel T, Grandaubert J, Hane JK, Hoede C, van de Wouw AP, Couloux A, Dominguez V, Anthouard V, Bally P, Bourras S, et al. 2011. Effector diversification within compartments of the *Leptosphaeria maculans* genome affected by Repeat-Induced Point mutations. *Nat Commun.* 2:202.

Rudd JJ, Kanyuka K, Hassani-Pak K, Derbyshire M, Andongabo A, Devonshire J, Lysenko A, Saqi M, Desai NM, Powers SJ, et al. 2015. Transcriptome and metabolite profiling of the infection cycle of *Zymoseptoria tritici* on wheat reveals a biphasic interaction with plant immunity involving differential pathogen chromosomal contributions and a variation on the hemibiotrophic lifestyle definition. *Plant Physiol.* 167:1158–1185.

Ryan CP, Brownlie JC, Whyard S. 2016. Hsp90 and physiological stress are linked to autonomous transposon mobility and heritable genetic change in nematodes. *Genome Biol Evol.* 8(12):3794–3805.

Saksouk N, Simboeck E, Déjardin J. 2015. Constitutive heterochromatin formation and transcription in mammals. *Epigenetics Chromatin* 8:3.

Sánchez-Vallet A, Fouché S, Fudal I, Hartmann FE, Soyer JL, Tellier A, Croll D. 2018. The genome biology of effector gene evolution in filamentous plant pathogens. *Annu Rev Phytopathol.* 56:21–40.

Saze H, Kakutani T. 2007. Heritable epigenetic mutation of a transposon-flanked *Arabidopsis* gene due to lack of the chromatin-remodeling factor DDM1. *EMBO J.* 26(15):3641–3652.

Schotanus K, Soyer JL, Connolly LR, Grandaubert J, Happel P, Smith KM, Freitag M, Stukenbrock EH. 2015. Histone modifications rather than the novel regional centromeres of *Zymoseptoria tritici* distinguish core and accessory chromosomes. *Epigenetics Chromatin* 8:41.

Seidl MF, Thomma B. 2017. Transposable elements direct the coevolution between plants and microbes. *Trends Genet.* 33(11):842–851.

Selker EU. 2002. Repeat-induced gene silencing in fungi. *Adv Genet.* 46:439–450.

Shetty NP, Mehrabi R, Lütken H, Haldrup A, Kema GHJ, Collinge DB, Jørgensen H. 2007. Role of hydrogen peroxide during the interaction between the hemibiotrophic fungal pathogen *Septoria tritici* and wheat. *New Phytol.* 174(3):637–647.

Shpyleva S, Melnyk S, Pavliv O, Pogribny I, Jill James S. 2018. Overexpression of LINE-1 retrotransposons in autism brain. *Mol Neurobiol.* 55(2):1740–1749.

Sienski G, Dönertas D, Brennecke J. 2012. Transcriptional silencing of transposons by Piwi and maelstrom and its impact on chromatin state and gene expression. *Cell* 151(5):964–980.

Skibbe DS, Doehlemann G, Fernandes J, Walbot V. 2010. Maize tumors caused by *Ustilago maydis* require organ-specific genes in host and pathogen. *Science* 328(5974):89–92.

Slotkin RK, Martienssen R. 2007. Transposable elements and the epigenetic regulation of the genome. *Nat Rev Genet.* 8(4):272–285.

Soyer JL, Ghalid ME, Glaser N, Ollivier B, Linglin J, Grandaubert J, Balesdent M-H, Connolly LR, Freitag M, Rouxel T, et al. 2014. Epigenetic control of effector gene expression in the plant pathogenic fungus *Leptosphaeria maculans*. *PLoS Genet.* 10(3):e1004227.

Soyer JL, Grandaubert J, Haueisen J, Schotanus K, Stukenbrock EH. 2019. *In planta* chromatin immunoprecipitation in *Zymoseptoria tritici* reveals chromatin-based regulation of putative effector gene expression. *bioRxiv.* 544627.

Soyer JL, Rouxel T, Fudal I. 2015. Chromatin-based control of effector gene expression in plant-associated fungi. *Curr Opin Plant Biol.* 26:51–56.

Stewart EL, Croll D, Lendenmann MH, Sanchez-Vallet A, Hartmann FE, Palma-Guerrero J, Ma X, McDonald BA. 2018. Quantitative trait locus mapping reveals complex genetic architecture of quantitative virulence in the wheat pathogen *Zymoseptoria tritici*. *Mol Plant Pathol.* 19(1):201–216.

Stewart EL, McDonald BA. 2014. Measuring quantitative virulence in the wheat pathogen *Zymoseptoria tritici* using high-throughput automated image analysis. *Phytopathology* 104(9):985–992.

Studer A, Zhao Q, Ross-Ibarra J, Doebley J. 2011. Identification of a functional transposon insertion in the maize domestication gene *tb1*. *Nat Genet.* 43(11):1160–1163.

Studt L, Rösler SM, Burkhardt I, Arndt B, Freitag M, Humpf H-U, Dickschat JS, Tudzynski B. 2016. Knock-down of the methyltransferase Kmt6 relieves H3K27me3 and results in induction of cryptic and otherwise silent secondary metabolite gene clusters in *Fusarium fujikuroi*. *Environ Microbiol.* 18(11):4037–4054.

Torriani SFF, Melichar JPE, Mills C, Pain N, Sierotzki H, Courbot M. 2015. *Zymoseptoria tritici*: a major threat to wheat production, integrated approaches to control. *Fungal Genet Biol.* 79:8–12.

Trivedi M, Shah J, Hodgson N, Byun H-M, Deth R. 2014. Morphine induces redox-based changes in global DNA methylation and retrotransposon transcription by inhibition of excitatory amino acid transporter type 3-mediated cysteine uptake. *Mol Pharmacol.* 85(5):747–757.

Trojer P, Reinberg D. 2007. Facultative heterochromatin: is there a distinctive molecular signature? *Mol Cell.* 28(1):1–13.

Van Meter M, Kashyap M, Rezazadeh S, Geneva AJ, Morello TD, Seluanov A, Gorbunova V. 2014. SIRT6 represses LINE1 retrotransposons by ribosylating KAP1 but this repression fails with stress and age. *Nat Commun.* 5:5011.

Vogel HJ. 1956. A convenient growth medium for Neurospora (medium N). *Microbial Genetics Bulletin* 13:42–43.

Voronova A, Belevich V, Jansons A, Rungis D. 2014. Stress-induced transcriptional activation of retrotransposon-like sequences in the Scots pine (*Pinus sylvestris* L.) genome. *Tree Genet Genomes.* 10(4):937–951.

Wang Q, Han C, Ferreira AO, Yu X, Ye W, Tripathy S, Kale SD, Gu B, Sheng Y, Sui Y, et al. 2011. Transcriptional programming and functional interactions within the *Phytophthora sojae* RXLR effector repertoire. *Plant Cell* 23(6):2064.

Wicker T, Sabot F, Hua-Van A, Bennetzen JL, Capy P, Chalhoub B, Flavell A, Leroy P, Morgante M, Panaud O, et al. 2007. A unified classification system for eukaryotic transposable elements. *Nat. Rev. Genet.* 8:973–982.

Williams BP, Pignatta D, Henikoff S, Gehring M. 2015. Methylation-sensitive expression of a DNA demethylase gene serves as an epigenetic rheostat. *PLoS Genet.* 11(3):e1005142.

Yasuda K, Ito M, Sugita T, Tsukiyama T, Saito H, Naito K, Teraishi M, Tanisaka T, Okumoto Y. 2013. Utilization of transposable element *mPing* as a novel genetic tool for modification of the stress response in rice. *Mol Breed.* 32:505–516.

Yoder JA, Walsh CP, Bestor TH. 1997. Cytosine methylation and the ecology of intragenomic parasites. *Trends Genet.* 13(8):335–340.

Zeng F, Cheng B. 2014. Transposable element insertion and epigenetic modification cause the multiallelic variation in the expression of FAE1 in *Sinapis alba. Plant Cell* 26(6):2648–2659.

Zhan J, Linde CC, Jürgens T, Merz U, Steinebrunner F, McDonald BA. 2005. Variation for neutral markers is correlated with variation for quantitative traits in the plant pathogenic fungus *Mycosphaerella graminicola. Mol Ecol.* 14(9):2683–2693.

Zhong Z, Marcel TC, Hartmann FE, Ma X, Plissonneau C, Zala M, Ducasse A, Confais J, Compain J, Lapalu N, et al. 2017. A small secreted protein in *Zymoseptoria tritici* is responsible for avirulence on wheat cultivars carrying the *Stb6* resistance gene. *New Phytol.* 214(2):619–631.

Zilberman D, Gehring M, Tran RK, Ballinger T, Henikoff S. 2007. Genome-wide analysis of *Arabidopsis thaliana* DNA methylation uncovers an interdependence between methylation and transcription. *Nat Genet.* 39(1):61–69.

Zovoilis A, Cifuentes-Rojas C, Chu H-P, Hernandez AJ, Lee JT. 2016. Destabilization of B2 RNA by EZH2 activates the stress response. *Cell* 167(7):1788–1802.e13.